ADVANCES IN INORGANIC CHEMISTRY, VOL. 36

MAGNETIC CIRCULAR DICHROISM OF HEMOPROTEINS

M. R. CHEESMAN,* C. GREENWOOD,** and A. J. THOMSON*

Centre for Metalloprotein Spectroscopy and Biology,
*School of Chemical Sciences and **School of Biological Sciences,
University of East Anglia, Norwich NR4 7TJ, England

I. Introduction

The study of the optical spectra of heme rings has a long history, beginning in 1886 with the classic studies of MacMunn (*1*), an Irish physician, who first observed with a hand spectroscope the sharp absorption bands of a pigment, later identified as myoglobin, in the flight muscle of the fly. Over 40 years were to elapse before Keilin, in Cambridge, carried out observations on a wide variety of cells and tissues with a microspectrophotometer (*2*). He recognized that the typical four-banded absorption spectrum was due to different pigments, which he called cytochromes *a*, *b*, and *c*, in descending order of their wavelengths. The first detailed discussion of the connection between the magnetic and optical properties of hemes was given by Williams in 1956 (*3*).

Interest in the potential application of magnetic circular dichroism (MCD) spectroscopy to the study of heme was kindled by a series of experiments carried out by Shashoua (*4*), who had constructed an instrument, using an electromagnet, to measure magnetically induced optical rotatory dispersion (MORD) spectra. He showed that relatively intense MORD signals from cytochrome *c* had a form that depended upon the oxidation state of the cytochrome. At the same time, P. J. Stephens, with A. D. Buckingham at Oxford, derived theoretical expressions that enabled MORD and MCD spectra to be analyzed and molecular parameters to be extracted (*5*). The need for high magnetic fields to improve the quality of spectra was met by Oxford Instruments, a small company set up by two technicians from the Clarendon Laboratory, Oxford, with the object of winding superconducting solenoids for research. These two developments, the theoretical understanding and the availability of high magnetic fields (5 T) from compact solenoids, led to the construction of an MCD spectrometer at the University of Virginia by P. N. Schatz, who had learned of its potential while on leave in Oxford. This collaboration between Schatz and Stephens led to the first analysis of the MORD and MCD spectra of diamagnetic metal porphyrins (*6*).

This was followed by a number of studies of the MCD spectra of hemoproteins, particularly from the Berkeley Laboratory of K. Sauer, using instrumentation designed and built by Dratz (*7, 8*). However, measurement could be made on samples only at room temperature or over a limited range, down to 77 K. The first report of the MCD spectra of hemoproteins frozen in an aqueous/sugar glass recorded at 15 K was by Briat and co-workers (*9*). The construction by Oxford Instruments of a split-coil superconducting magnet, in which the sample could be immersed in a liquid helium bath, necessitated the development of optical windows that remained strain free and capable of propagating circularly polarized light at 4.2 K. This led to the ability to make measurements routinely on samples of hemoproteins over the temperature range 1.5–300 K and up to fields of 6–7 T, and opened the way for the measurement for the first time of MCD magnetization curves of metalloproteins and hence the methodology for the study of the ground-state magnetic properties of individual heme centers in proteins (*10*). The first MCD spectra of hemoproteins in the near-infrared region were reported in 1973 by Cheng *et al.* (*11*). They showed that the form of the MCD spectra of the charge-transfer (CT) bands were different for high- and low-spin hemes.

It is now possible to measure the MCD spectra of hemoproteins in a solution of water and cryoprotectant mixtures over the wavelength range 195–5000 nm at magnetic fields up to 10 T, with good sample

temperature control over the range 1.5–300 K. Although MCD studies in the vacuum ultraviolet region have been carried out using laboratory-based instruments and synchrotron sources, no reports have appeared of the spectra of hemoproteins in this wavelength region.

This article describes the progress made over the last 10 years in studies of the MCD spectra of heme models and proteins. The review is not exhaustive but draws primarily upon the work carried out at the University of East Anglia by the authors and their co-workers. This work began in 1970 with the first report of the MCD spectrum of the 695-nm band of cytochrome *c* (*12*), but the primary focus has been the development of methods of performing MCD studies on aqueous solutions of proteins at temperatures down to 1.5 K. The original impetus was to probe the nature of the alleged magnetic coupling in cytochrome *c* oxidase between heme a_3 and Cu_B in the oxidized resting state of this enzyme. This is still today an unsolved problem, but we have been able to demonstrate the direct interaction between these two centers in the cyanide-inhibited state of the enzyme (*13, 14*). This quest has led to the development of MCD methodology and to the mapping out of the low-temperature MCD characteristics of a wide range of hemoproteins in the several spin states of ferrous, ferric, and ferryl hemes. The need to devise more highly selective methods of probing the electronic properties of metal centers in complex multicentered proteins gave rise to the first experiments using MCD signals to detect ground-state microwave resonance, a technique called, whimsically, paramagnetic resonance by optical detection, or PROD (*15*). This review outlines briefly this progress, which owes a debt to the early work of Williams (*3*) pointing out the significance of the relationship between the magnetic and optical properties of the heme group and to the interest of one of us in the use of spectroscopy with polarized light. This originated in the laboratory of R. J. P. Williams in the early 1960s with the construction of a microspectrophotometer for the measurement of the polarized single-crystal spectra of hemoproteins (*16, 17*). During the same period, discussions with P. J. Stephens about using low-temperature MCD spectroscopy for the study of paramagnetic metal centers in proteins clearly identified the potential. However, these studies only became possible and routine when suitable cryostats and magnets had been developed.

II. Principles of MCD Spectroscopy Applied to Hemes

The MCD spectrum is a measure of the difference between the absorption of right- and left-circularly polarized light as a function of the

wavelength of the measuring light when the sample is placed in a magnetic field applied parallel to the direction of propagation of the light beam. Transitions between electronic states can only be induced by circularly polarized light provided that the component of the electronic orbital angular momentum in the direction of the magnetic field changes by either -1 or $+1$ for the absorption of right- or left-circularly polarized light, respectively. The application of a magnetic field leads to the lifting of electronic orbital and spin degeneracies and to the mixing of electronic states. MCD spectroscopy enables the optical transitions between Zeeman sublevels of ground and excited states to be observed with circularly polarized light, even though the Zeeman splitting may be orders of magnitude smaller than the linewidth of the transition.

There are three distinct effects caused by the application of a magnetic field, namely, the Zeeman splitting of ground and/or excited states, the field-induced mixing of states, and a change in population of molecules over a set of Zeeman split sublevels of a ground state. These give rise, respectively, to the A term, the B term and the C term. Illustrations and discussions of these phenomena are given fully elsewhere (*18–20*).

The optical spectra of porphyrins are readily understood in terms of the four-orbital model of Goutermann and Wagnière (*21*), which unites the Hückel model with the free-electron and cyclic polyene models (*22*). The highest occupied molecular orbitals (HOMOs) and lowest unoccupied molecular orbitals (LUMOs) of an aromatic 18-π electron system belong to the irreducible representations a_{2u}, a_{1u}, and e_g of the point group D_{4h}, when the porphyrin molecule has a four-fold axis of symmetry (Fig. 1). The HOMOs have four nodes and the LUMOs have five nodes, making them analogous to the orbitals of the free-electron model with components of orbital angular momentum of ± 4 and ± 5 units about the four-fold axis. The four one-electron transitions $a_{1u} \rightarrow e_g^x$, $a_{1u} \rightarrow e_g^y$, $a_{2u} \rightarrow e_g^x$, and $a_{2u} \rightarrow e_g^y$ have counterparts $\pm 4 \rightarrow \pm 5$ and $\pm 4 \rightarrow \pm 5$. These give rise to two double degenerate transitions in D_{4h}. The two excited states of E_u symmetry that arise from these configurations are not pure but are mixed under the influence of interelectronic repulsion.

The absorption spectrum of a diamagnetic metalloporphyrin consists of two electronic transitions, the Q-band (or α-band) in the region 550–600 nm, of lower intensity, corresponding to the mixture of one-electron transitions that involve partial cancallation of the dipole moments, and the other, the B-band (or Soret band), between ~380 and 450 nm, of high intensity, which comprises the one-electron transition

involving the sum of the dipole moments. The excited state of the *Q*-band has, in the limit of complete mixing, a high orbital moment, $\pm 9\beta$, whereas that of the *B*-band has a low moment, $\pm 1\beta$. The MCD spectrum of a diamagnetic metalloporphyrin shows an intense *A* term in

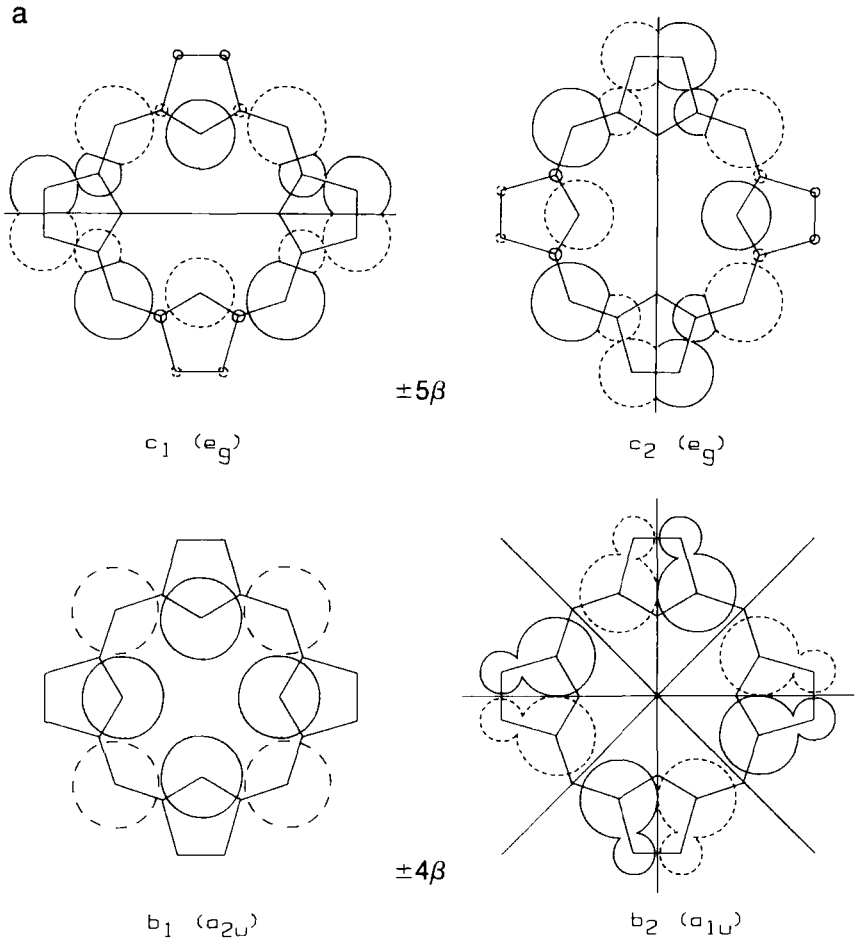

FIG. 1. (a) HOMOs and LUMOs of 18-π electron porphyrin ring system. The orbital coefficients are proportional to the sizes of the circles. Circles with solid or dashed lines indicate sign of wavefunction. Nodes are drawn in heavy lines (*21*). Also indicated are the components of the orbital angular momentum perpendicular to the ring as predicted by the free-electron theory (22). (b) Energy states of a diamagnetic metalloporphyrin in the presence of a *z*-directed magnetic field and the Zeeman transitions between the ground and two excited E_u states. The form of the MCD and absorption spectrum is sketched below, with left (L) and right (R) circularly polarized light. Here *A* is absorbance and $\Delta A = A_L - A_R$; *B* is the magnetic field and λ is the wavelength.

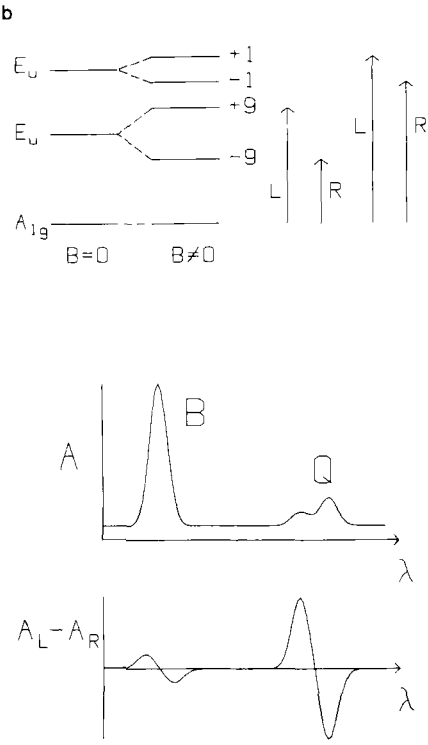

FIG. 1. (*continued*)

the Q-band and a weak A term in the B band because of the higher magnetic moment of the former compared with the latter (Fig. 1). As configuration interaction between the B- and Q-bands varies the intensity ratio of the absorption spectrum changes, as does the magnitude of the A term.

When the x, y degeneracy of the porphyrin ring is lifted, both Q- and B-bands may be split into two components that are x and y polarized. The degeneracy is lifted in metal-free porphyrins by the two protons in the ring center, by unsymmetrical substitution of the porphyrin exocyclic ring or by partial reduction of one or more of the pyrrole rings to generate unsymmetrical rings such as chlorins. The MCD spectrum in these cases gives rise to two bands of opposite sign arising from the x- and y-polarized transitions (*23, 24*). When the separation of these two transitions is greater than the bandwidth, the MCD signals arise from the field-induced mixing of the x- and y-polarized transitions by the z-directed magnetic field, and hence are B terms.

The presence of a transition metal ion in the center of the porphyrin ring introduces several complexities into the optical and the MCD spectra. The metal ion provides energy levels of the d electrons and additional optical transitions can be observed. These can be classified broadly into metal localized d–d and charge transfer from metal d to porphyrin π (e_g) (MLCT) or vice versa (LMCT) (*25*).The states arising from all these configurations are mixed by the action of low-symmetry crystal field components and spin orbit coupling. If the metal ion possesses unpaired electrons in its ground state, then the MCD spectrum of all the optical transitions may become temperature dependent, arising from C terms. The porphyrin π–π^* transitions can only give temperature-dependent C-term intensity in the MCD spectrum if the porphyrin states become mixed with the paramagnetic metal d-configurations. This invariably occurs in the case of iron porphyrin, in nickel tetrapyrrole (F-430) (*26*), and in cobalt(II) corrin (*27*). However, little work has been reported on the presence of MCD C terms in the spectra of other metalloporphyrin ring systems. Copper(II) porphyrin apparently does not show temperature dependence in the MCD spectrum of the π–π^* transitions (*28*).

In the case of a paramagnet with a ground-state spin $S = 1/2$, the MCD intensity depends linearly upon the applied magnetic field, B_0, and inversely upon the absolute temperature, T, provided that kT is greater than $g\beta B_0$, the Zeeman splitting of the ground state (Fig. 2a). This is the Curie law region of the magnetization curve. However, at high fields and ultralow temperature ($T < 10$ K), the MCD signal will become independent of temperature and magnetic field (provided that A and B terms are insignificant). The sample is then saturated, all paramagnetic molecules populating only the lower of the two Zeeman sublevels of the ground state. The curve represents the MCD magnetization. The absolute value of the MCD intensity at the saturation limit depends upon a number of factors, including the ground-state g-value, and the absolute transition-moment intensity, which in turn depends upon the nature of the excited state. However, the steepness of the initial or Curie law slope depends upon the ground state Zeeman splitting only. In simple cases, the intercept value, I, defined as the ratio of the saturation limit to the Curie law slope, is related to the ground state g value. For an isotropic g factor $I = 1/g$ and for a completely axial ground state with $g_\parallel \neq 0$ and $g_\perp = 0$, $I = 1.5/g_\parallel$ (*29*).

When the ground-state spin is greater than $S = 1/2$, then the MCD magnetization curves may become complex, so that curves measured at different temperatures do not overlap (Figure 2b). This situation has been called a "nested" set (*10*) and arises because of field-induced mix-

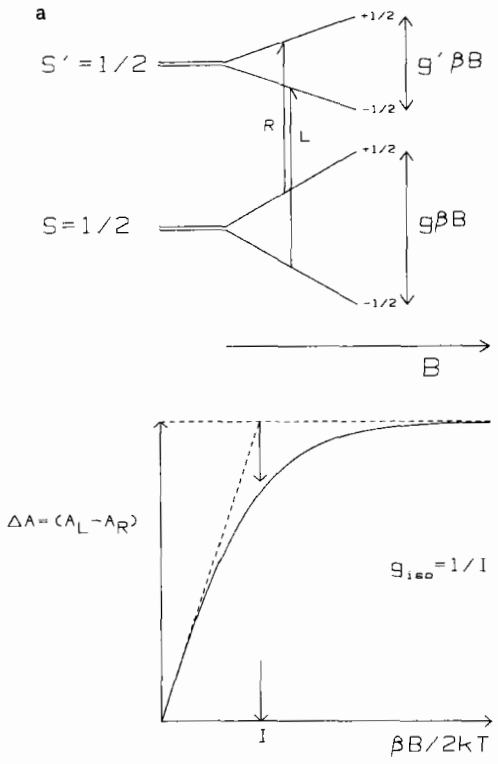

FIG. 2. (a) Ground and excited states of a spin $S = 1/2$ in a magnetic field, B, and MCD magnetization curve; I = intercept value; (b) MCD magnetization curve for a ground state with spin $S = 2$ subject to an axial zero-field splitting $D = +10$ cm^{-1}, and rhombicity $E = 0$, xy polarized transition, at various temperatures as indicated, and magnetic field between 0–5 T. B, Magnetic field; β, Bohr magneton; k, Boltzmann's constant; T, temperature.

ing of energy levels lying close to the ground state or to thermal population of low-energy sublevels. The detailed analysis of such curves requires computer-generated simulations, which are not necessarily unambiguous.

The realization that measurements of the intensity of an MCD spectrum into the region where it is nonlinear in field and temperature could be analyzed to yield ground-state g values enabled the magnetic properties of individual paramagnetic centers in a multicentered metalloprotein to be probed for the first time (*10*). The detailed analysis of the temperature dependence of the MCD spectrum at magnetic field strengths that are within the linear limit enable the zero-field splitting

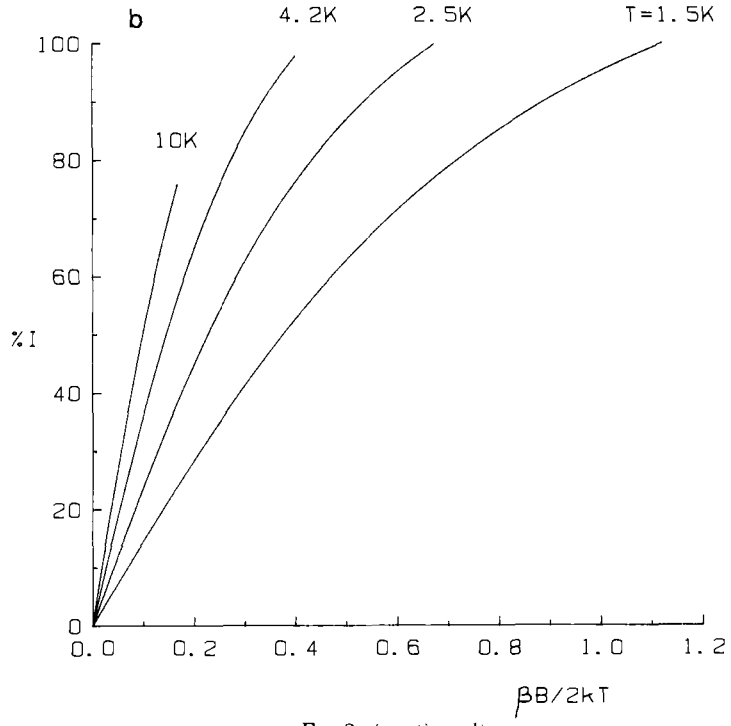

FIG. 2. (*continued*)

parameters of ground states with spins greater than 1/2 to be determined (*29*).

III. Optical and MCD Spectra of Ferrous and Ferric Hemes

A. INTRODUCTION

The optical and MCD spectra of the heme group vary markedly depending upon the nature of the porphyrin ring, upon the spin and oxidation state of the iron at the center of the ring, and upon the nature of the axial ligand to the metal ion. To illustrate the dependence of the MCD spectra upon the spin and oxidation state of the metal ion, a selection of spectra of the high- and low-spin states of ferrous and ferric hemoproteins containing protoporphyrin IX ring is shown in Figs. 3 and 4. The spectra, recorded at room temperature and 4.2 K, are strikingly dependent upon the magnetic state of the metal

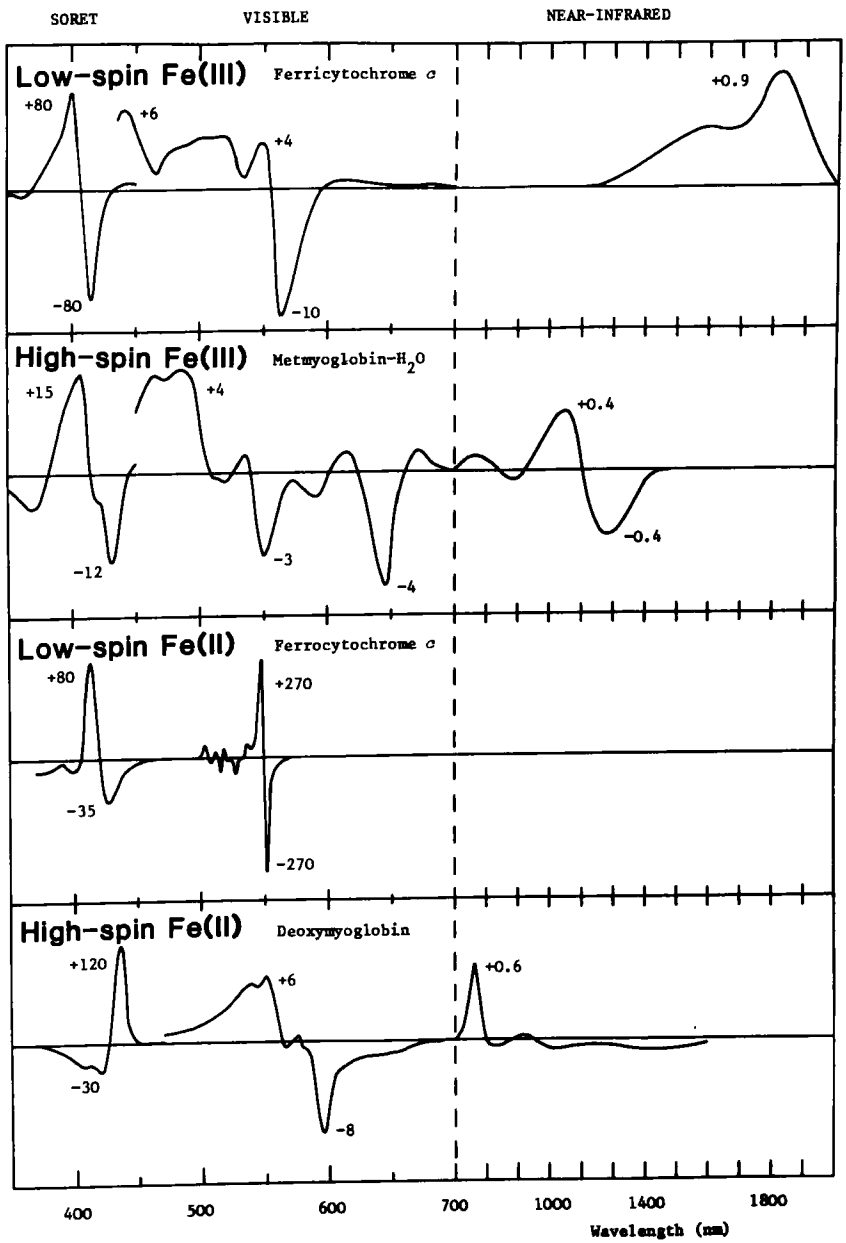

FIG. 3. MCD spectra recorded at room temperature of low-spin ferric heme (ferricytochrome *c*, horse heart), high-spin ferric heme (metmyoglobin–H_2O), low-spin ferrous heme (ferrocytochrome *c*), and high-spin ferrous heme (deoxymyoglobin). Intensities are indicated at the prominent peak and trough wavelengths in units of M^{-1} cm^{-1} T^{-1}, where T = Tesla [taken from N. Foote, Ph.D. Thesis, UEA (1984)].

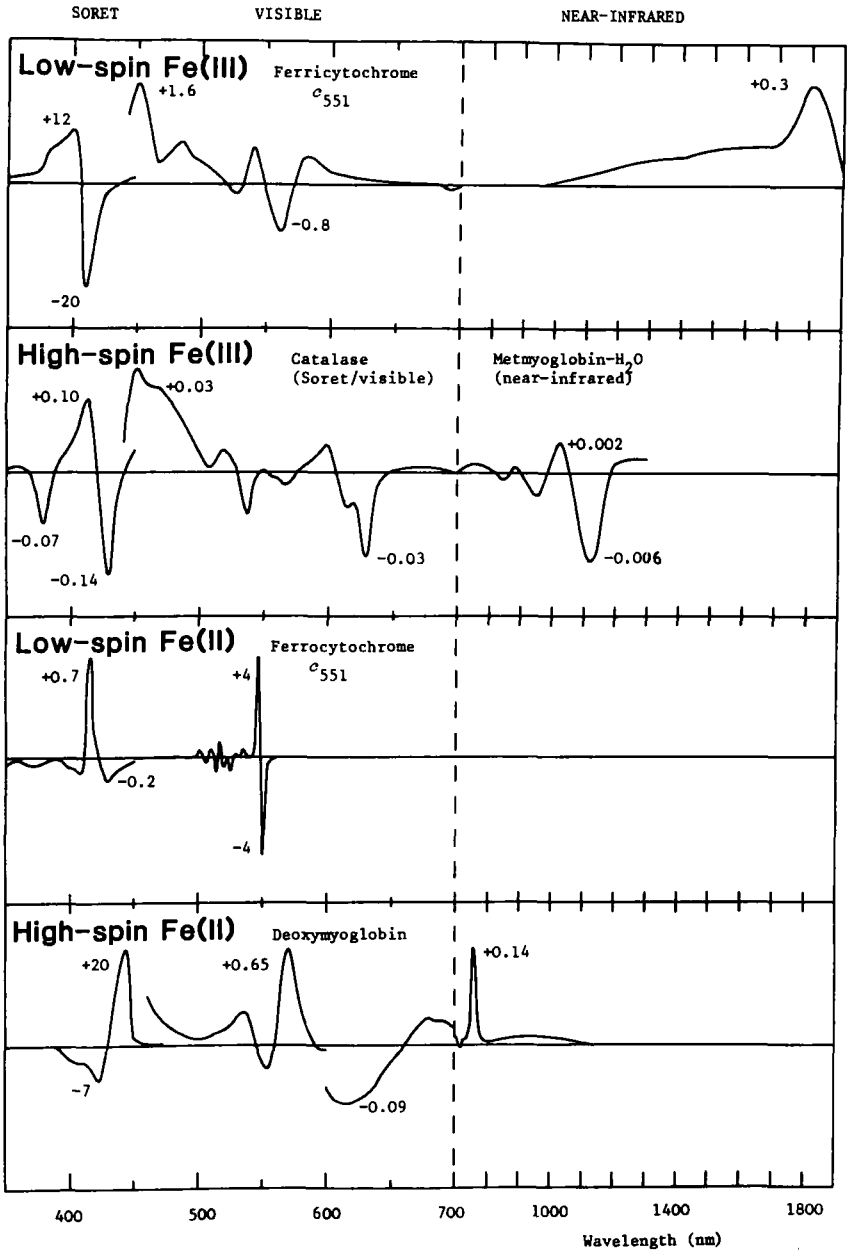

FIG. 4. MCD spectra recorded at 4.2 K and 5 T of low-spin ferric heme (ferricytochrome c_{551}), high-spin ferric heme (catalase and metmyoglobin–H_2O), low-spin ferrous heme (ferricytochrome c_{551}), and high-spin ferrous heme (deoxymyoglobin). Intensities are indicated at the major peaks and troughs in units of mM^{-1} cm^{-1} [taken from N. Foote, Ph.D. Thesis, UEA (1984)].

ion, as indeed are the optical spectra. The theoretical basis of this correlation and the assignment of these spectra are now well established. As a consequence, the spectra can be used with some confidence for structural assignments. In the following sections we discuss the main features of the spectra and then show how information relevant to the structure of heme within protein environments can be read from them.

B. Ferrous Hemes

1. Low-Spin Heme

Ferrocytochrome *c* is in the low-spin, ferrous state and hence is diamagnetic. The MCD features (Figs. 3 and 4) arise from the porphyrin *Q*- and *B*-bands and contain only *A* and *B* term intensity. The MCD intensity increases by a factor of ~2 both in the *Q*- and *B*-bands between room temperature and 4.2 K. This is due entirely to the narrowing of the bandwidths on cooling. The magnitude of the MCD *A* term is very sensitive to linewidth ($\alpha\ 1/\Gamma^2$, where Γ is the width of the band at half the height). However, band sharpening is largely complete on cooling from room temperature to 100 K. The lack of *C* term intensity can be shown by the absence of temperature dependence over the range 1.5–100 K. The MCD spectrum in both the *B*- and *Q*-bands is dominated by the *A* term intensity, which arises from the orbital degeneracy of the π–π^* states, ^1E_u. The free-electron model of Simpson predicts magnetic moments for the *B*- and *Q*-bands of 1β and 9β, respectively (*22*). Calculations of the ratios $A/D(Q) = 1/2b_{11}$ and $A/D(B) = 1/2b_{22}$ (where $b_{11} = 9$ and $b_{22} = 1$ and *D* is the dipole strength) predict that *A*/*D* is nine times greater for the *Q*-band than for the *B*-band (*6*). The experimental data indeed show that the *Q*-band intensity is more intense than that of the *B*-band. Analysis by curve fitting of the *A* term of the *Q*-band of cytochrome *c* gives a value for b_{11} of 7.9β (*7, 30*), reasonably close to the free-electron prediction. Detailed molecular obital calculations have also confirmed a high value for the magnetic moment of the *Q*-band excited state (*31*). The *Q*-band at both room temperature and 4.2 K shows well-resolved vibronic structure on the high-energy side arising from excited-state vibrational frequencies of the porphyrin ring. The form of the MCD spectrum is not strongly dependent upon the nature of the axial ligands to the ferrous(II) ion. The MCD spectra of bis(histidine)-coordinated low-spin ferrous heme are very similar in form (*32*).

The *d*–*d* states of low-spin d^6 ions, such as Fe(II), are well studied in simple octahedral complexes. Two spin-allowed transitions, $^1A_{1g} \rightarrow$

$^1T_{1g}$, $^1T_{2g}$, are observed with ε values typically ~50–100 M^{-1} cm^{-1}. These transitions have been located in the CD and MCD spectra of cytochrome *c* (*33, 34*) and in the spectrum of cytochrome *a* in cytochrome *c* oxidase (*35*). A number of bands, not shown in Figs. 3 and 4, are found between 600 and 1000 nm in the spectra of cytochrome *c* with $\varepsilon \sim 200$ M^{-1} cm^{-1} and assigned, tentatively, to the $^1A_{1g} \rightarrow {}^1E_g$ component of the lowest *d–d* transition. In the MCD spectrum of reduced cytochrome *c* oxidase, no bands are present in this region when cytochrome a_3 is bound by CN^-, but characteristic *d–d* bands are seen in the CO complex. Hence it appears that coordination by CN^-/histidine and bis(histidine) shifts the *d–d* states of low-spin Fe(II) below the porphyrin π–π^* states. Methionine/histidine and CO/histidine coordination of Fe(II) does permit observation of the *d* states to a longer wavelength than the *Q*-band. However, because the heme is diamagnetic, the MCD spectrum gives no sensitivity advantage in locating these transitions. A detailed absorption, MCD, and CD study of the NIR spectrum of oxyhemoglobin assigns the four bands observed between 1200 and 600 nm both to *d–d* and porphyrin-to-metal CT, the oxygen π orbitals being strongly mixed with the *d* orbitals (*36*).

2. *High-Spin Ferrous Heme*

The ground state of high-spin ferrous heme contains four unpaired electrons, giving rise to a spin state $S = 2$. The orbital component of this state is quite unclear, even of any well-studied hemoproteins. However, it is possible that a number of orbital components of the $S = 2$ state, $^5B_2$ and ^5E, as well as other spin states, such as ^3E and ^1A, lie within about 1000 cm^{-1} of the ground state (*34, 37*). The MCD spectra of high-spin ferrous heme are in striking contrast to those of the low-spin state. The spectra in the *Q*- and *B*-bands are strongly temperature dependent; for example, the positive peak at 550 nm has $\Delta\varepsilon = 30$ M^{-1} cm^{-1} at 5 T and room temperature, which rises to $\Delta\varepsilon = 650$ M^{-1} at the same field and 4.2 K. The variation of the intensity with field and temperature is complex (Fig. 2b), giving rise to a nested set of magnetization curves. The complexity arises predominantly from second-order Zeeman mixing of zero-field components within the ground-state quintet and also at higher temperatures from variations in thermal population over these components. The MCD magnetization characteristics have not yet been successfully fitted to theoretical expressions. However, the form of these plots varies among different species of high-spin ferrous hemes, showing differences between the zero-field splitting parameters (*38*).

The region of the MCD spectrum between 650 and 1400 nm contains several electronic transitions that have also been located by single-crystal spectroscopy (*34, 39*). In deoxyhemoglobin, four transitions to longer wavelength of the *Q*-bands have been identified. Three of them have been assigned as CT transitions: $d_{xz} \rightarrow e_g$ (π^*) at 10,900 cm^{-1}, a_{2u} (π) $\rightarrow d_{yz}$ at 13,300 cm^{-1}, and a_{1u} (π) $\rightarrow d_{yz}$ at 14,900 cm^{-1}, and the last as a d–d transition, $d_{xz} \rightarrow d_z^2$ at 12,300 cm^{-1}.

Several studies have been made of the MCD spectra of the high-spin ferrous state formed by low-temperature photolysis of CO and O_2-bound hemoproteins, particularly myoglobin, hemoglobin, and cytochrome *c* oxidase (*38–40*). In the case of the reversible oxygen carriers, the photolysed species is high-spin ferrous but with different ground-state zero-field parameters and shifted NIR bands. This is interpreted as an inability of the frozen hemoprotein to relax from the ligand-bound to the deoxy form. The photolysed form generated at 4.2 K can be identified with the so-called "quickly reacting" form first identified by Gibson (*41*). This species is not generated by the photolysis of CO-bound cytochrome *c* oxidase, suggesting that the oxygen-binding heme, cytochrome a_3, does not undergo a significant change in conformation between the high- and low-spin ferrous states (*38*).

C. Ferric Hemes

The spectra of both high- and low-spin states of ferric heme consist of a porphyrin π–π^* transition plus porphyrin (π)-to-metal CT transitions (Figs. 3 and 4). The MCD spectrum of low-spin Fe(III) protoheme IX in the *Q*- and *B*-band regions is due primarily to porphyrin-localized transitions, although there are undoubtedly CT states overlapping them. The NIR region shows a band of characteristic shape that arises from the CT transition, porphyrin (π) to Fe(III) $d_{xz,yz}$. The energy of this transition is sensitive to the energies of the Fe(III) *d* orbitals and as a consequence changes in axial ligation of the iron cause considerable variation in the wavelength of this band. In special cases, charge transfer from axial ligand to ferric ion have been observed. The "695"-nm band of ferricytochrome *c* is due to CT from methionine sulfur orbitals to Fe(III) *d* orbitals (*42*). By contrast, the MCD spectra of high-spin Fe(III) hemes are more complex. The basic reasons underlying this were given by Williams and co-workers (*43*). They pointed out that the two allowed CT transitions from porphyrin-to-metal a_{1u}, a_{2u} (π) to $e_g(d_{xz,yz})$, which gave rise to two excited E_u states, are at higher energy compared with the low-spin state. Therefore, the CT configurations are strongly mixed with the *B*- and *Q*-states, also of E_u symmetry. This

severely disrupts the typical B- and Q-band pattern of the porphyrin optical spectrum, yielding four excited ^6E_u states, which fall approximately in the wavelength regions 700–1000, 600–650, 500–600, and 350–450 nm. As a consequence, the MCD spectrum is exceedingly complex, with a form much more dependent upon the nature of the axial ligation than are the spectra of states in which the $\pi-\pi^*$ and CT configurations are less strongly mixed. Nevertheless, the lowest energy transition between 700 and 1000 nm moves systematically with variation in axial ligation. Hence it has been used to diagnose variations in axial ligation of the heme group.

The form of the MCD spectrum of the low- and high-spin CT bands was first described by Stephens and co-workers (*11, 44*) (Fig. 5). Assuming that the heme ring approximates to C_{4v} symmetry, the low-spin ground state has a configuration $e^3(d_{xz,yz})$, giving rise to a state ^2E that is split by spin–orbit coupling and a rhombic field into two Kramer's doublets. The two CT configurations, $a_{1u}^1e_g^4$ and $a_{2u}^1e_g^4$, give rise to excited states of symmetry $^2A_{1u}$ and $^2A_{2u}$. On application of a magnetic field, both ground and excited states undergo a Zeeman splitting. The transition from the lower compound of the ground state is left

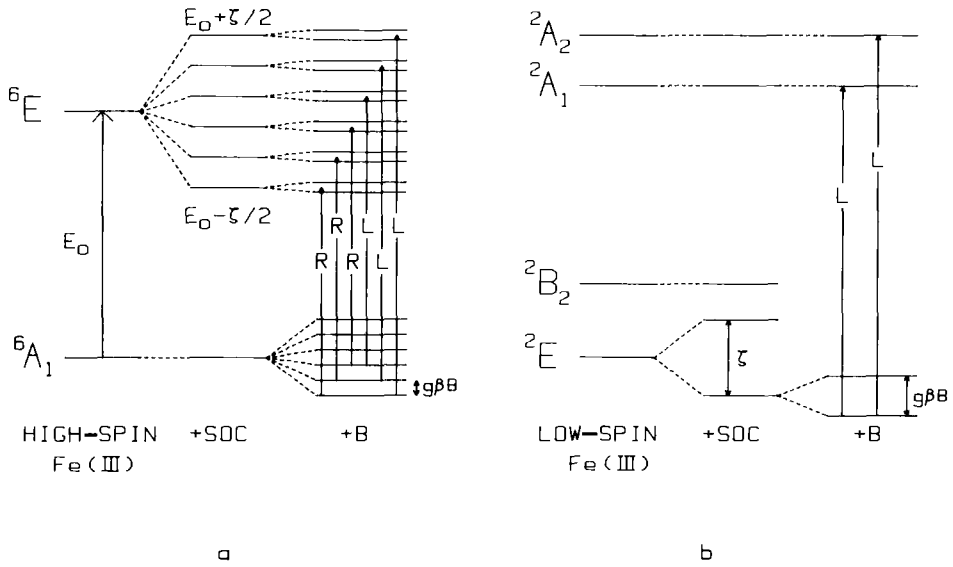

FIG. 5. Ground and excited states of (a) high-spin and (b) low-spin ferric hemes, including the effects of spin–orbit coupling (SOC) and a z-directed magnetic field, B. The selection rules for right (R) and left (L) circularly polarized light are indicated (adapted from Ref. *45*).

circularly polarized, giving rise to the positive MCD band. The high-spin ground state contains the half-filled d shell and therefore transforms as $^6A_1$. The two CT configurations give rise to two states, ^6E. Under the influence of first-order spin–orbit coupling, each state splits into six pairs of Kramer's doublets separated in total by ζ, the spin–orbit coupling constant. On application of a magnetic field, the ground-state spin degeneracy is removed and each Kramer's doublet of the CT state is split. The selection rules for circularly polarized light are shown in Fig. 5. It can be seen that the sign of the C term varies, being negative for the lower spin–orbit components and of opposite sign for the upper components. Consequently, the MCD changes sign through the band, giving the appearance of an A term but having a temperature dependent on oppositely signed C terms predominating at 1.5 K.

An important difference between the MCD spectra of high- and low-spin ferric heme is the temperature variation of the MCD intensities. Because both states are paramagnetic, the MCD spectra are temperature dependent. However, although the absolute MCD intensities of both spin states are comparable at room temperature (Fig. 3), at 4.2 K the MCD intensities of the low-spin ferric heme are a factor of ~100 greater than that of the high-spin ferric heme. The reason for this is the magnitude of the orbital magnetic moment of the ground state. The high-spin ferric ion has almost zero orbital moment, but a high-spin moment, whereas the low-spin ferric ion has a ground-state doublet that arises by low-symmetry distortion and spin–orbital coupling from the $^2T_2$ state, which has first-order orbital moment $L = 1$. It is a general property of MCD spectra that transitions from a spin-only ground state will give rise to A terms if there is no first-order spin–orbit coupling in the excited state. The C term intensity appears as spin–orbit coupling increases, as shown in Fig. 5. In the excited ^6E states of high-spin ferric heme, the orbital moment arises primarily from the angular momentum of the porphyrin orbitals, whereas the spin moment comes from the metal. Spin–orbit coupling between moments on different centers is weaker than that between moments on a single atom. Hence the effective spin–orbit coupling in the excited states of high-spin ferric heme is low. This results in the low intensity of the MCD transition. Nevertheless, the MCD spectra of high-spin Fe(III) heme at 4.2 K are dominated by C terms and the spectra are temperature dependent (*45*).

However, it is important to be aware of the large difference in MCD intensity between the high- and low-spin forms of heme, because the MCD spectra of the latter invariably dominate the spectrum at 4.2 K. For this reason, amounts of low-spin ferric heme of ~1% in a sample of

hemoprotein or other protein can dominate the spectrum. It has proved difficult to obtain MCD spectra of high-spin ferric heme that are totally free from contamination by low-spin heme. The spectral region between 700 and 1000 nm can be a useful window in which to make measurements, because few low-spin ferric hemes have any optical transitions in this region.

1. Axial Ligand Assignment of Low-Spin Ferric Hemes

The low-spin state of ferric hemes can, with one exception, only be brought about if both axial positions of the coordination shell of the Fe(III) ion are occupied with strong field ligands. The axial ligands can be side chains of amino acid residues of the protein binding the heme or a combination of one such side chain and one exogenous donor, such as HO^- or H_2O. The single exception to this rule, namely, an example of a low-spin ferric heme with a single axial ligand, is the SH^- derivative of the model complex Fe(III) octaethylporphine (OEP) (*46*). In the low-spin state with both axial positions occupied, the heme group usually functions are a reversible electron carrier, the redox transition Fe(III) $\leftrightarrow$ Fe(II) being rapid because little electronic reorganization occurs at the metal center. The redox potentials of heme centers in proteins are often pH dependent and the molecular origin of this variation is of interest. The linking of a redox process with a change in pK_a of a group buried in a protein is one essential component of a redox-driven proton pump. The identification of the molecular events in such processes is still obscure although of central importance in bioenergetics. Hence the ability to be able to identify axial ligand type and to follow axial ligand changes as a function of pH and redox state is important.

Surprisingly, the unambiguous identification of the axial ligation state of hemoproteins using spectroscopic methods has proved problematical. The electronic transitions of the porphyrin ring dominate the visible and UV spectra. It is necessary to use techniques that monitor the properties of the ferric ion. Hence the EPR spectra that arise from the unpaired d electron in the t_{2g} subshell do depend upon the axial ligation state, and were early used as the basis of the method of heme axial ligand assignment devised by Blumberg and Peisach and enshrined in the so-called truth table (*47*). The NIR CT bands of low-spin Fe(III) heme vary substantially in wavelength as a function of the energies of the acceptor d orbitals, $d_{xz,yz}$, and consequently of the axial ligands of the ferric ion (Fig. 6). Hence the energy of the NIR CT band can also be used as an indicator of the nature of the axial ligand provided a sufficiently wide range of hemes of known axial ligation type are available to calibrate the scale (*48*).

Williams (*43*) first drew attention to this potential and succeeded in locating the CT bands of low-spin ferric hemoproteins principally by measuring their polarized single-crystal spectra (*17*). However, some of these CT bands, it is now clear, lie at wavelengths between 800 and 3000 nm. The spectral region beyond ~1400 nm contains the absorption bands arising from the vibrational overtones C—H, N—H, and O—H (Fig. 6a). By exchanging the protons with deuterons, the overtone absorption can be considerably reduced, and by using careful difference spectroscopy the broad CT bands can be located. However, in many proteins, complete exchange of all protons does not take place

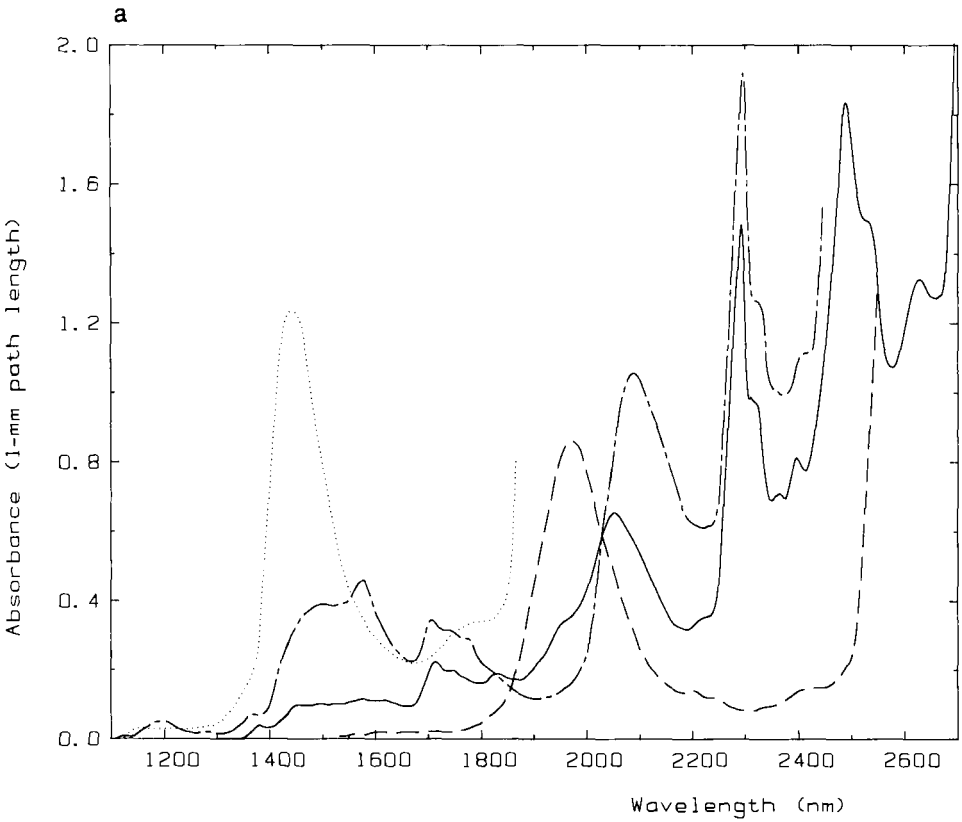

FIG. 6. (a) Absorption spectra in the near-infrared region between 1000 and 3000 nm of some solvents used for the measurement of the MCD spectra of metalloproteins. Path length is 1 mm. (·····), H_2O; (—·—), ethanediol; (– – –), D_2O; and (——), 75% deuteroethanediol (unpublished work of J. Peterson). (b) Examples of MCD spectra of low-spin ferric hemes in the NIR region measured at 4.2 K and the 5-T field. (Top) methionine–histidine; (bottom) bis(histidine) coordination. Intensity is given by $\Delta\varepsilon = \varepsilon_L - \varepsilon_R$.

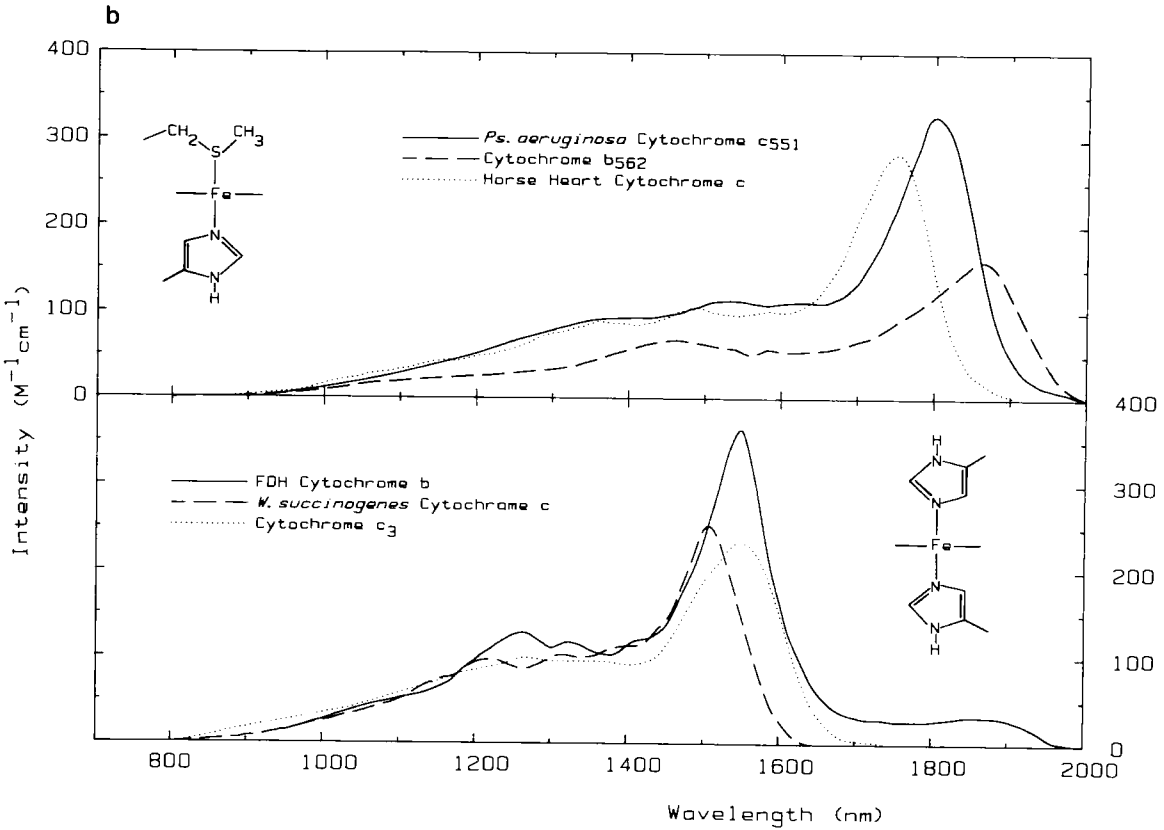

FIG. 6. (*continued*)

because of inaccessibility to solvent. It is for these reasons that the NIR MCD spectroscopy is particularly valuable for the location of electronic transitions in the region of 1400–3000 nm. MCD intensity depends upon the Zeeman splitting of either the ground or excited state and upon field-induced mixing of states. These effects depend, in turn, upon the g factor and the magneton, i.e., the Bohr magneton for electronic states and the nuclear magneton for vibrational states. Because the latter is at least three orders of magnitude smaller than the former, the MCD intensities of vibrational transitions are several orders of magnitude weaker than electronic transitions (*49*). Consequently, the MCD spectra in this wavelength region locate only the electronic transitions. The sample must be dissolved in D_2O or a suitable organic solvent to reduce the overtone absorption and to permit transmission of sufficient photon intensity to enable the MCD spectrum to be measured with acceptable signal-to-noise ratios. The MCD spectrum is the most ready method to locate the low-energy CT bands of low-spin ferric hemoproteins. It has the added advantage that measurements can be made with samples either at room temperature or at a low temperature, enabling changes in spin equilibria or axial ligation to be monitored as a function of temperature. Because the EPR spectra of low-spin ferric hemes can be detected only at liquid helium temperatures, this is an important advantage. Figure 6b shows some examples of the NIR MCD CT spectra of low-spin Fe(III) hemoproteins with bis(histidine) and methionine–histidine coordination.

In addition to giving the means to locate NIR CT bands, the MCD spectrum contains useful additional information. The sign of the MCD band depends upon the absolute sign of the ground state g_z component. In all cases we have studied, the NIR CT gives rise to a positive C term, implying that the absolute value of g_z is positive. We have also shown that the intensity of the MCD spectrum depends upon the rhombic distortion experienced by the Fe(III) ion, and this, in turn, can be related to the orientation of axial ligands (*50*).

a. Charge-Transfer Energy as a Function of Axial Ligation. The electronic energy levels of low-spin Fe(III) protoporphyrin IX relevant to the interpretation of the EPR, optical, and MCD spectra are illustrated in Fig. 7. The allowed porphyrin-to-Fe(III) CT one-electron transitions are $a_{1u} \rightarrow e_g(d_{xz,yz})$ and $a_{2u} \rightarrow e_g(d_{xz,yz})$. Both gain intensity by borrowing from the allowed B- and Q-bands via the mixing of the $e_g(d_{xz,yz})$ metal orbitals with the $e_g(\pi^*)$ unoccupied orbitals. It has been estimated that the mixing coefficient is ~5% (*50*). The intensity of the NIR CT bands are of the order of ε ~200–300 M^{-1} cm^{-1}, whereas

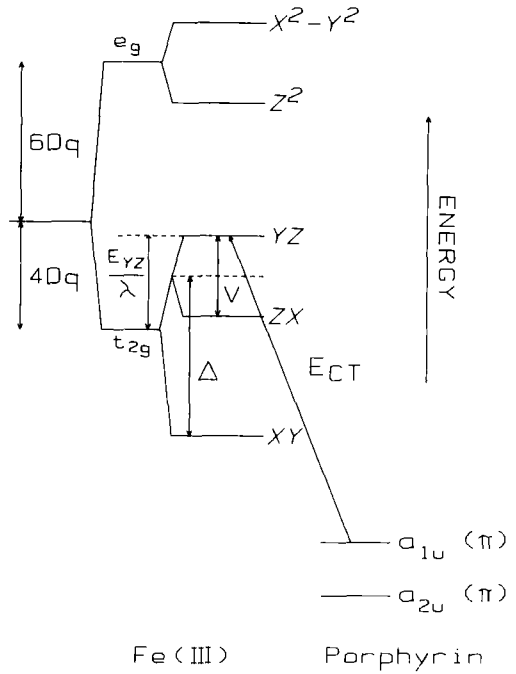

FIG. 7. The energy levels of low-spin ferric heme for the assignment of the EPR and CT bands. The levels on the left are the metal *d* orbitals and on the right are the porphyrin HOMOs.

typical *Q*-band intensities are $\varepsilon \sim 10^4\ M^{-1}\ \text{cm}^{-1}$ and *B*-bands have $\varepsilon \sim 10^5\ M^{-1}\ \text{cm}^{-1}$.

Polarized single-crystal spectra have shown that the broad CT bands in the NIR region are exclusively polarized in the heme plane (*17*). This is required because all the intensity is borrowed from the heme $\pi-\pi^*$ transitions, which are also established to be exclusively in-plane polarized. There has been uncertainty whether one or both CT transitions, $a_{1u} \rightarrow e_g$ and $a_{2u} \rightarrow e_g$, lie within the rather broad envelope of the NIR absorption band. This has been a difficult question to resolve because both transitions are predicted to be in-plane polarized and to give positive MCD bands. The NIR spectrum of met-Mb-CN at 4.2 K has well-resolved structure (*51*). It was therefore suggested that the partially resolved structure to high energy arises from vibronic levels. Recent evidence obtained by a comparison of the NIR MCD spectra of low-spin complexes of Fe(III) OEP and Fe(III) tetraphenylporphine (TPP) strongly suggests that only one transition, namely, $a_{1u} \rightarrow e_g$, is

present between 800 and 3000 nm in the NIR spectra of Fe(III) protoporphyrin IX derivatives (*52*).

The NIR MCD spectra of the bis(imidazole) complexes of Fe(III) OEP and Fe(III) TPP are shown in Fig. 8. In the former case the typical band shape of bis-ligated Fe(III) protoporphyrin IX is observed. However, in the case of Fe(III) TPP, an additional electronic transition is present at 1100 nm. Therefore we assign the major features as the two one-electron transitions. Inspection of the electron density distribution of the a_{1u} and a_{2u} orbitals around the porphyrin ring (Fig. 1) shows the reason for the differences between the energies of the $a_{1u} \rightarrow e_g$ and $a_{2u} \rightarrow e_g$ transitions in the OEP and TPP rings. The a_{1u} orbital has nodal planes running through the methine bridges, whereas the a_{2u} orbital has significant electron density at the bridges. Hence substitution of methine H atoms by phenyl groups, as in TPP compared with OEP, will lead to changes in the energy of the a_{2u} orbital but leave the energy of the other orbital, a_{1u}, unchanged. Therefore, phenyl substitution at the porphyrin methine bridge is expected to leave the energy of the $a_{1u} \rightarrow$

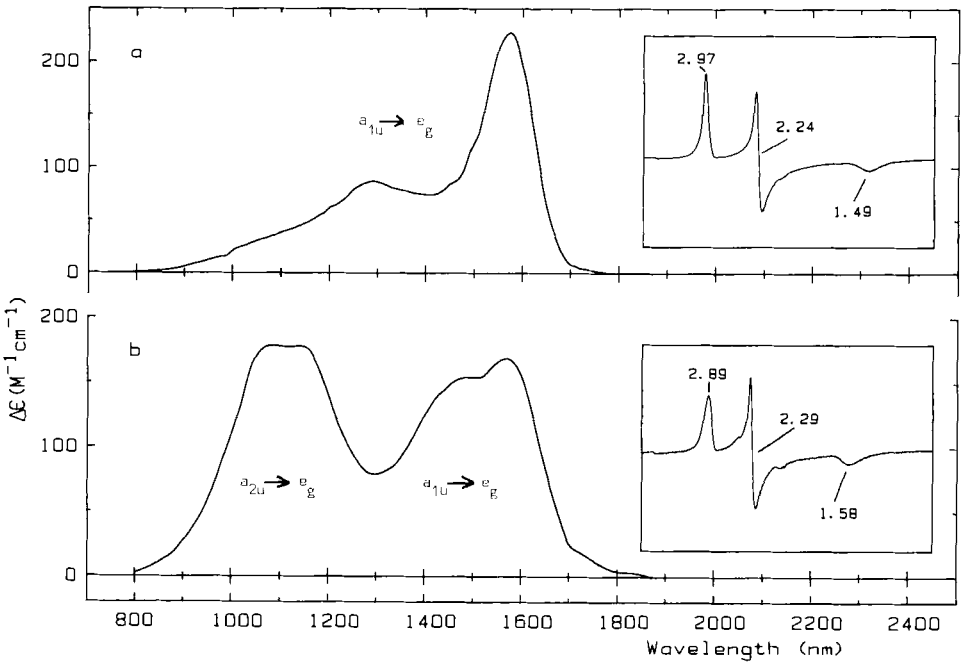

FIG. 8. A comparison of the NIR MCD spectra at 4.2 K and 5 T of the CT bands of (a) bis(imidazole)–Fe(III) OEP and (b) bis(imidazole)–Fe(III) TPP in $CH_2Cl_2/(C_2H_5)_2O$ (2 : 1 v/v). The EPR spectra shown as an insert were measured at X-band and 10 K.

e_g transition unchanged but to shift the energy of the $a_{2u} \rightarrow e_g$ transition. This difference gives a criterion for assignment of the transition as shown in Fig. 8.

Measurements have been made of the transition energies of the $a_{1u} \rightarrow e_g$ CT transition of a wide range of low-spin Fe(III) heme models and proteins in order to establish whether unique axial ligand assignments can be made on the basis of band positions alone (*48*). The bands have been located using low-temperature (4.2 K) MCD spectroscopy, but in all cases the EPR spectra of the same sample have been recorded. In order to measure the MCD spectrum at ultra-low temperature, aqueous solutions are diluted to 50% v/v with a cryoprotectant solvent, typically ethanediol or glycerol. This enables a glass with good optical transmission to be obtained. In order to check that no changes have been induced by the solvent, the EPR spectrum of the sample is measured both before and after addition of the cryoprotectant. In some cases, changes in axial ligation are induced by addition of cryoprotectant. The EPR spectrum also provides a second set of parameters, namely, the g values, and the axial (Δ) and rhombic (V) crystal-field distortion parameters, which can be derived from them. These parameters are also diagnostic of axial ligand type, although not necessarily uniquely. Ligand assignment based upon both EPR and MCD parameters helps to lessen ambiguities.

These data and the conclusions derived from them apply to heme groups of the protoporphyrin IX ring and the heme *a* ring. The results also apply to Fe(III) OEP models. The porphyrin ring systems, which do not conform to these rules, are the partially reduced rings such as haem d and Fe(III) TPP. It seems probable that other partially reduced porphyrin rings as found in chlorin, bacteriochlorin, and siroheme will not show NIR CT bands in this region. However, much further experimental work is required to establish where the CT bands lie in these systems.

The results obtained can be collected into three groups, depending upon the nature of the axial ligand. Of the 21 amino acids, only four provide side chains with donor atoms of sufficiently high ligand field strength to bring about the low-spin state of Fe(III) heme when biscoordinated. They are lysine ($-NH_2$), histidine ($\gtrless N$), cysteine ($-S^-$), and methionine ($>S$). Histidinate derived from histidine by loss of the N-1 proton can also ligate. The NIR CT band reveals that this deprotonation process can take place at physiologically relevant pH values (*53–55*). Four potential low-spin axial ligands lead to the expectation that up to 10 different pairs of axial ligation could be discovered in low-spin Fe(III) hemoproteins. Only four examples have now been defi-

nitely established; they are methionine–histidine (crystallographically in cytochrome *c* and cytochrome b_{562}) (*53*), histidine–histidine (crystal structure of cytochrome b_5 and cytochrome c_3), lysine–histidine [spectroscopic evidence on cytochrome *f* (*56*) and the high-pH form of cytochrome *c*, horse heart] (*57*), and, most recently, bis(methionine) (MCD and EPR evidence on bacterioferritin) (*58*).

The ranges in which E_{CT} falls for these and other ligation states are illustrated in Fig. 9, which summarizes the experimental and the predicted energies of the major peaks of the porphyrin-to-Fe(III) CT bands. The experimental data, plotted as solid-line rectangles, come

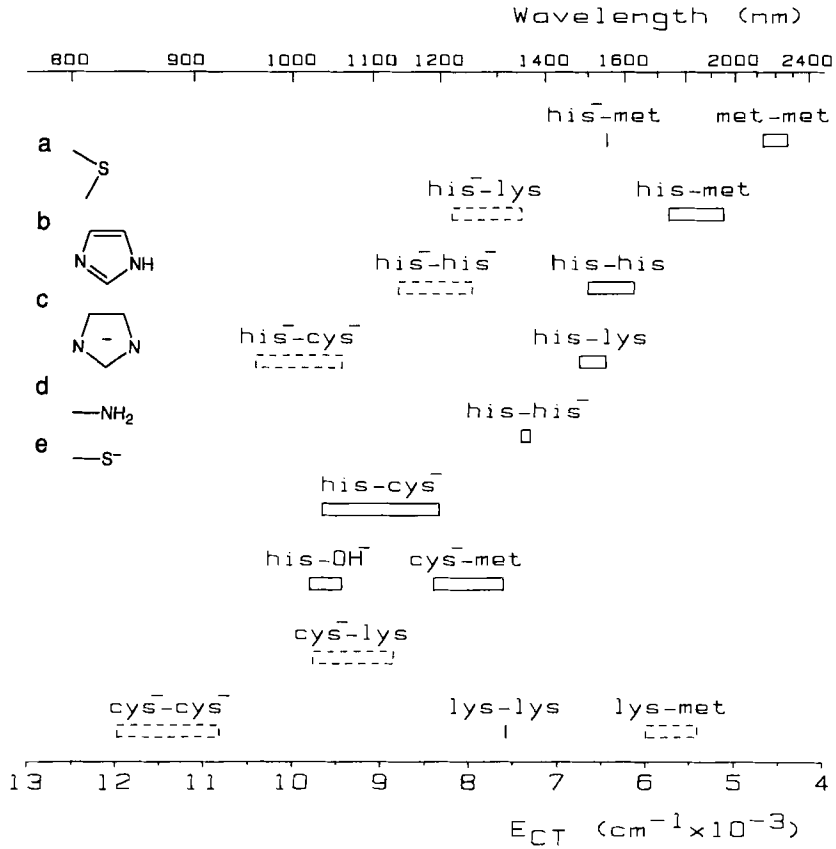

FIG. 9. The energies of the CT bands of bis-coordinated low-spin ferric protoheme IX complexes determined at 4.2 K by NIR MCD spectroscopy. The boxes with solid lines indicate the range of values obtained experimentally either from proteins or models. The boxes with broken lines show the energies predicted from the additivity rule (see text). The coordinating groups are (a) Met, (b) His, (c) His^-, (d) Lys, and (e) Cys.

from measurements on proteins of known structure or model bis-liganded heme complexes. E_{CT} varies somewhat for a given axial ligation set as a function of the protein, presumably because of local structural variations, such as ligand orientation, H bonding, and the polarity of the heme pocket. Where a single line in Fig. 9 is shown, only one example of such coordination has been discovered. Using the values of E_{CT} for the structurally characterized complexes, it is clear that an additivity rule exists as follows. Each ligand type can be assigned an energy such that the addition of this parameter for each ligand yields E_{CT}. Thus the parameters are Met (2250 cm^{-1}), His (3200 cm^{-1}), Lys (3750 cm^{-1}), His^- (4100 cm^{-1}), and Cys (6000 cm^{-1}). Hence bis(Met) ligation generates a band at $E_{CT} \approx 4500$ cm^{-1} (2200 nm), and bis(His) ligation generates a band at $E_{CT} \approx 6400$ cm^{-1} (1560 nm). The CT band for bis(Cys) coordination is predicted to lie at 12,000 cm^{-1} (830 nm). The data points predicted according to this procedure are shown as rectangles with dashed lines. Models of these need to be examined to verify the validity of the prediction.

The maximum spread of E_{CT} is from ~4500 to ~12,000 cm^{-1}. It is clear from Fig. 9 that it is possible to assign ligand pairs for protoheme IX unambiguously on the basis of E_{CT} alone, only in the case of Met-Met and Cys-Cys, which have unique values of E_{CT}. The rest suffer overlap to a greater or lesser extent. However, in combination with EPR g values, remarkably little ambiguity occurs; Gadsby and Thomson (*48*) discuss this aspect in detail. The identification of His^- can be made if the deprotonation process $His \rightleftharpoons His^-$ can be detected within the pH range of protein stability. The EPR g values undergo a distinctive change in concert with the move of E_{CT} to higher energy on deprotonation. The distinction between His-His and His-Lys is ambiguous without the EPR spectrum. There are only limited data on lysine–histidine coordination, but the g_z values are high ($g_z = 3.51$), and of gaussian shape in the case of cytochrome f (*56*). Although bis(His) coordination can also generate high g_z values if the rhombic distortion, V, is low, the lineshape of g_z becomes ramp shaped. The other potential source of ambiguity is expected to be the distinction between His-Met and Lys-Met. Because the latter coordination has not been modeled, there are no EPR data on which to base a distinction. Clearly this is urgently needed. Similarly, the distinction between $His\text{-}Cys^-$ and Cys^--Lys is a potential ambiguity, but again no models of the latter coordination are yet available.

By the judicious use of E_{CT} values together with EPR g values and where possible the utilization of additional constraints from, for example, protein sequence data, the axial ligation states can usually be

established with certainty or narrowed to a limited choice of possibilities. A recent case is the demonstration that the heme group in bacterioferritin from several sources, including *Escherichia coli, Pseudomonas aeruginosa, Azotobacter vinelandii,* and *Rhodopseudomonas sphaeroides* (*58*), is liganded by two methionine side chains, a unique form of bis-axial heme ligation. The value of E_{CT} was confirmed by the synthesis of suitable model bis(thioether) complexes, that is, bis(tetrahydrothiophene) Fe(III) OEP (*52*) (Fig. 10). This is an example of the discovery of novel and unexpected heme ligation by NIR MCD and EPR spectroscopy.

b. Dependence of MCD Intensity on Rhombic Distortion at Fe(III) Ion. It has been possible to demonstrate experimentally and to justify theoretically that the intensity of the MCD spectrum of the NIR CT band of low-spin ferric hemes depends upon the rhombic distortion at the Fe(III) site (*59*). This in turn leads to some conclusions about the relative orientation of axial ligands necessary to generate crystal fields of low rhombic distortion at the metal center.

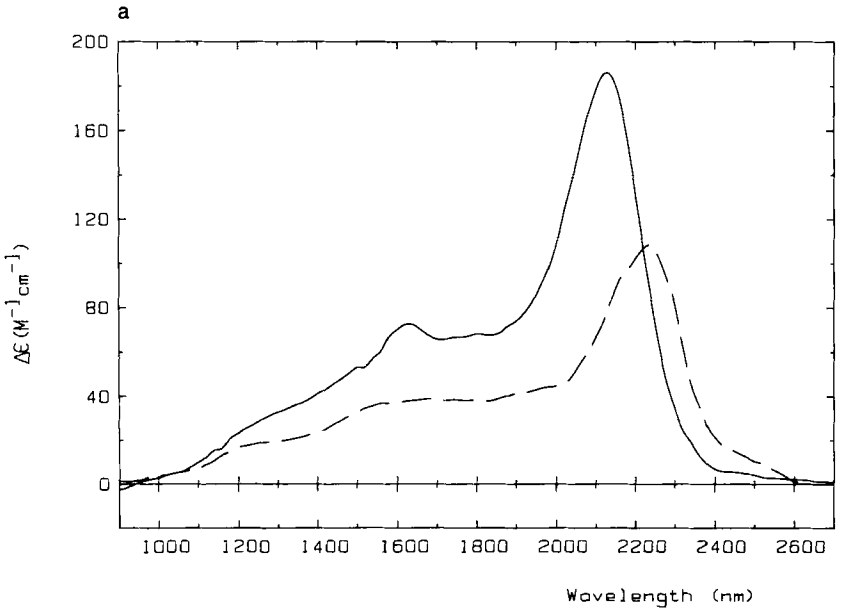

FIG. 10. (a) A comparison between the NIR MCD spectra of bacterioferritin (*Pseudomonas aeruginosa;* dashed line) and the model complex [bis(tetrahydrothiophene)–Fe(III) OEP; solid line] in $CH_2Cl_2/(C_2H_5)_2O$ (2 : 1 v/v) at 4.2 K and 5 T. (b) EPR spectra of the two species shown in (a) (unpublished data of J. McKnight, M. R. Cheesman, C. A. Reed, and A. J. Thomson).

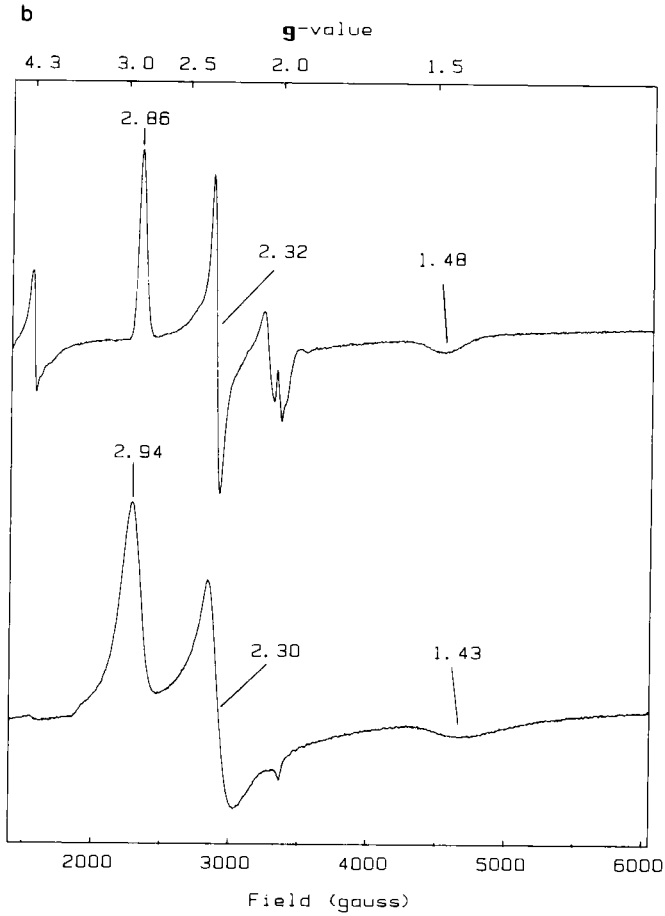

FIG. 10. (*continued*)

Using the theoretical model given earlier for the source of the intensity of the porphyrin-to-metal CT band, $a_{1u} \rightarrow e_g$, it can be shown that the dipole strength, D, of the CT transition is given by

$$D = \alpha^2(a^2 + b^2)m^2$$

where α is the coefficient that mixes the $e_g(d_{xz,yz})$ state and the $e_g(\pi^*)$ porphyrin state, a and b are the coefficients of the d_{xz} and d_{yz} orbitals in the ground-state Kramer's doublet, and m is the one-electron matrix element of the electric dipole operator. The MCD spectrum at low temperature is dominated by the contribution from the C term, which

is expressed by

$$C = g_z \alpha^2 abm^2$$

where g_z is the z component of the g tensor of the ground-state Kramer's doublet.

The ratio C/D is given by $g_z ab/(a^2 + b^2)$. When the Fe(III) ion has a four-fold axis of symmetry, then $x \equiv y$, and V, the rhombic distortion parameter, will be zero. The unpaired electron is equally shared between the d_{xz} and d_{yz} orbital and, as a consequence, $a = b$. In this case $C/D = g_z/2$, which is the maximum value it can have (*59*). However, in the limit of maximum rhombic distortion, $x \neq y$, the degeneracy of the $d_{xz,yz}$ pair is lifted, and the electron becomes localized in one orbital, say, d_{yz}. At the limit, one of the coefficients, say a, becomes zero. Hence the C term intensity and the MCD signal go to zero. However, because $a^2 + b^2 = 1 - c^2$, the dipole strength, D, remains unaffected. This argument shows that though the intensity of the absorption spectrum is unaffected by rhombic distortion at the Fe(III) ion, the MCD intensity is sensitive to variations in V. The exact dependence of the MCD C term intensity upon the rhombic distortion parameter V is shown in Fig. 11. In the limit that $V = 0$, the transition $a_{1u} \rightarrow e_g(d_{xz,yz})$ is equally x and y polarized. However, as V tends to infinity, the CT transition, say $a_{1u} \rightarrow e_g(d_{yz})$ becomes purely y polarized. A one-dimensional transition has no MCD intensity because the absorption of circularly polarized radiation requires two transitions polarized perpendicular to the applied field.

In the limit of complete axiality the MCD intensity is high, and the EPR spectrum assumes rather special properties. As $V \rightarrow 0$, then $g_\parallel \rightarrow 4.0$ and $g_\perp \rightarrow 0$, assuming that the t_{2g}^5 configuration has $S = 1/2$ and $L = 1$. If the orbital moment of the ground state is less than 1, the limit of $g_\parallel$ will fall below 4.0. As $g_\parallel$ approaches a limit, the lineshape of the EPR spectrum becomes highly asymmetric and ramp shaped (*60*). The g strain contributes the major broadening process to the g-value lineshapes. Because $g_\parallel$ cannot exceed g_{max}, the line cannot be broadened on the low-field edge and the line is truncated on this side. Such spectra have been called "highly anisotropic low spin" (or HALS). However, this term is misleading and should more properly be rephrased as "highly axial low spin" (HALS).

In a series of model bis(imidazole) complexes, Gadsby and Thomson (*61*) showed that as the EPR spectra became HALS, the MCD intensity of the NIR CT band increased in intensity. The dependence of $\Delta\varepsilon$ upon V has been explored in detail and verified with a range of low-spin

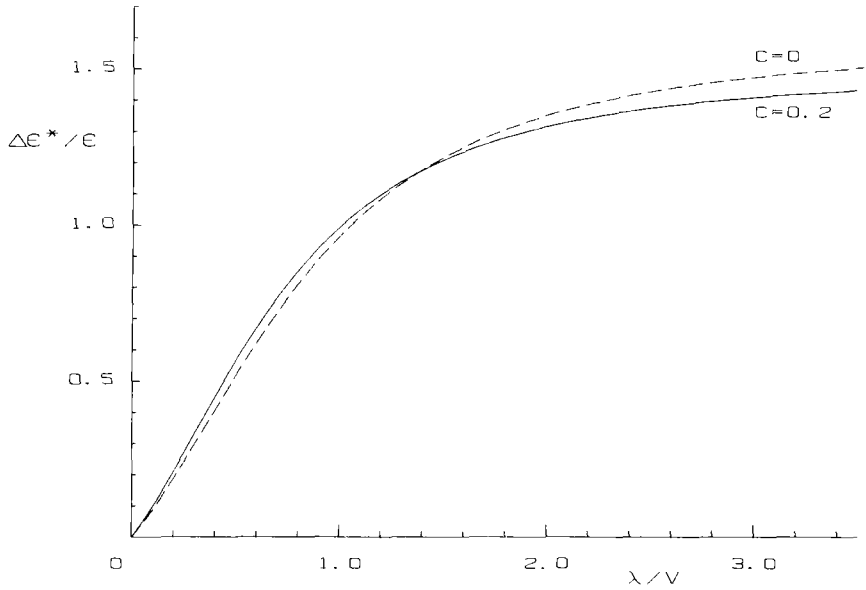

FIG. 11. The calculated dependence of the MCD intensity upon the rhombic distortion parameter, V, at low-spin Fe(III) in heme. $\Delta\varepsilon^*$ is the MCD intensity at 4.2 K and 5 T corrected to be linear in-field, ε is the extinction coefficient in isotropic light, and λ is the spin–orbit coupling constant of Fe(III) (*60*); c is the coefficient of the $3d_{xy}$ orbital in the ground state.

heme models and proteins (*59*). The crystal structure of the model complex bis(2-methyl-imidazole) Fe(III) OEP shows that the planes of the two axial ligands are 89° to one another (*62*). Apparently the steric bulk of the methyl groups in the 2-position causes the imidazole plane to swing into a position of minimum electron density around the heme plane. It is not clear why the ligands adopt a 90° or staggered orientation rather than the eclipsed or 180° orientation. This model fits well a number of protein examples in which it is clear that bis(histidine) coordination is present with a 90° orientation of the two axial ligands (see Section III,D,2).

2. *Axial Ligand Assignments of High-Spin Ferric Heme*

The variation in the energy of the longest wavelength CT band can be used to follow axial ligand variation of high-spin ferric heme as has been done for low-spin heme (*63*). The longest wavelength CT band lies in the region of ~800–1200 nm and therefore can be located readily by absorption spectroscopy. MCD provides a useful check on the assign-

ment of the band to the high-spin state of the heme because it has the characteristic bisignate shape. Rather few examples have been studied, so the spectroscopic scale is not well calibrated. The spectra for metmyoglobin show that E_{CT} moves from 1000 nm (H_2O), to 920 nm ($HCOO^-$), and 850 nm (F^-). The NIR MCD spectra of cytochrome c' isolated from photosynthetic bacteria reveal interesting pH dependences of the heme spectra. The structure of cytochrome c' is known to be five-coordinate at pH 7.0, giving a pure $S = 5/2$, high-spin spectra judged by the EPR signals. On raising the pH, the EPR signal becomes characteristic of quantum-mechanical mixed-spin species ($S = 5/2$ and 3/2). The NIR CT band of cytochrome c' from *Rhodopseudomonas rubrum* shifts about 2000 cm^{-1} to the blue on passing through a pK_a value of 8.4. The authors of this work proposed that a carboxylate side chain becomes bound to the iron of the heme at higher pH (*63*). Another possibility is that the heme remains five-coordinate and the proximal histidine ligand deprotonates to give histidinate. This would provide a species with a strong axial field superimposed on the high-spin state, the condition required according to Maltempo (*64*) to induce the mixed-spin state.

D. Applications

In this section we outline briefly some of the useful structural data that have been obtained by the measurement of the NIR CT spectra of hemoproteins using MCD and EPR spectroscopy.

1. Deprotonation of Histidine Groups Bound to Low-Spin Ferric Heme

The imidazole ring of histidine shows, in aqueous solution, two pK_a processes at 7.0 and >14.0. When the ring is ligated via N-3 to the iron atom of the heme ring, the first pK_a process is blocked. However, an interesting question concerns the value of the pK_a of the N-1 atom when the imidazole ring is bound to heme. The deprotonation process leading to the histidinate group gives two observable changes in the electronic properties of the low-spin Fe(III) ion. First, the NIR CT band moves by ~1000 cm^{-1} to the blue (Fig. 12a), and second, the g values change in a systematic way from $g = 3.03$, 2.29, and 1.50 to $g = 2.82$, 2.29, and 1.69 on deprotonation of the imidazole group bound to heme in leghemoglobin a (soybean) and from $g = 3.03$, 2.18, and 1.40 to $g = 2.79$, 2.26, and 1.67 in cytochrome b_{562} (*E. coli*) (*53*) (Fig. 12b). These two parameters taken together are unambiguous evidence for the deprotonation process and enable the pK_a values to be determined. The

pK_a values of several different systems studied by us are summarized in Fig. 13.

It is clear that ligation of histidine via N-3 to the Fe(III) ion lowers the aqueous pK_a value by about 3 units. This is presumably a polarization by the metal ion transmitted via the aromatic ring of histidine. Further lowering of this pK_a can only be brought about by the juxtaposition of basic residues in the protein close to the N-1 atom. Two mechanisms are proposed for the cases of leghemoglobin *a* and cytochrome b_{562}. The first involves a charge-relay process via the distal histidine group and possibly a carboxylate anion. It is known that the leghemoglobin pocket has a high affinity in the ferric state for anionic ligands such as picolinate and acetate. The stabilization of the anionic imidazolate is perhaps unsurprising, but the mechanism has been obscure in spite of the existence of a crystal structure. The case of cyto-

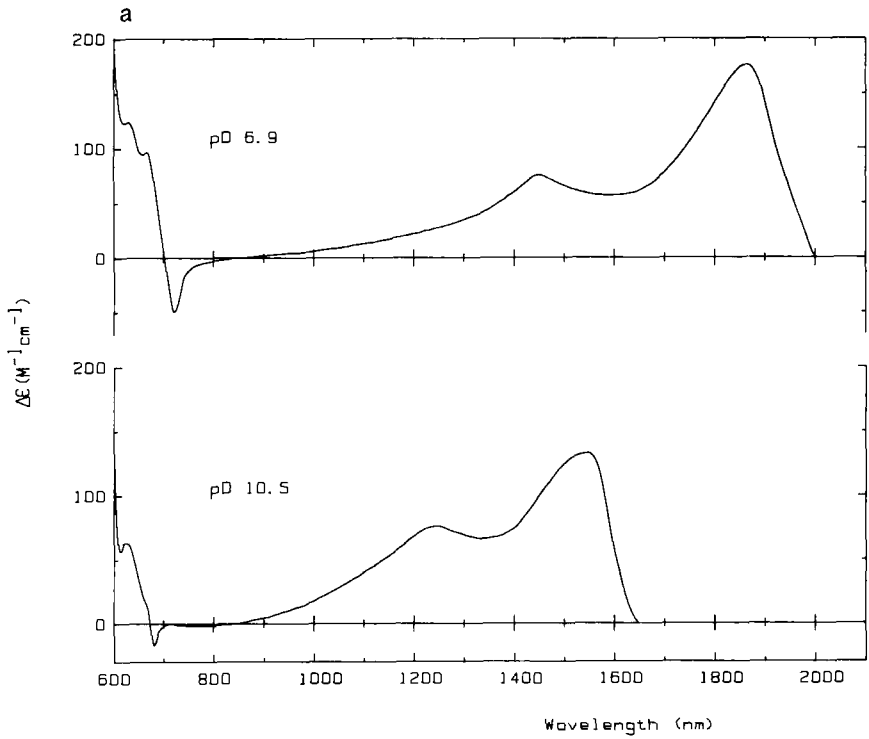

FIG. 12. (a) The NIR MCD spectra measured at 4.2 K and 5 T of ferricytochrome b_{562} (*E. coli*) at pD 6.9 and 10.5. The energy shift is due to the deprotonation of N-3 of the proximal histidine residue, to generate the histidinate group. (b) The EPR spectra of ferricytochrome b_{562} (*E. coli*) at pD 6.9 and 10.5, measured at X-band and 10 K (*53*).

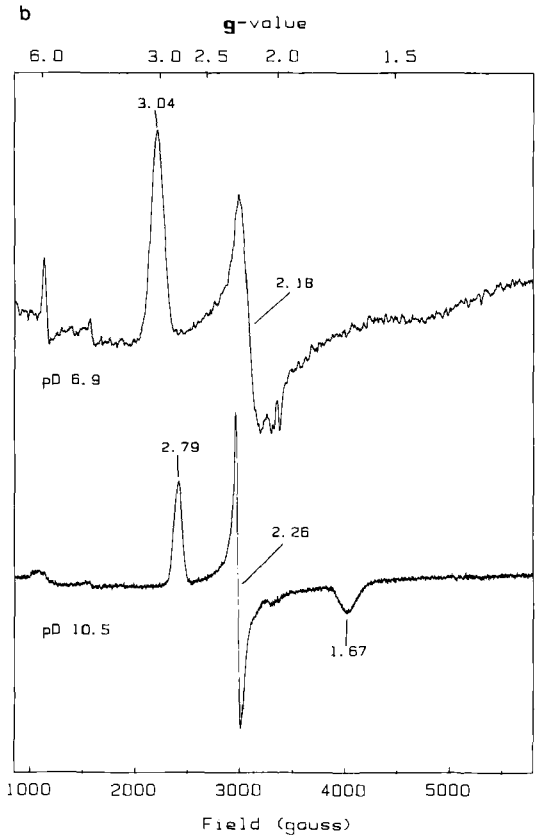

FIG. 12. *(continued)*

chrome b_{562} is quite clear and appears to involve an organic residue that can H-bond to the proximal histidine group to promote deprotonation. Thus we are led to the conclusion that the pK_a of the N-1 atom of histidine can be shifted by up to 7 units, from 14.0 to ~7.0, by a combination of effects, including polarization by Fe(III) and the juxtaposition of suitable basic residues close to the histidine ring.

The deprotonation process has not been studied in the Fe(II) states of these proteins partly because there are no spectroscopic parameters of the ferrous state capable of following histidine deprotonation. However, it seems likely that on reducing Fe(III) to Fe(II) the polarizing power of the metal ion will drop and the pK_a value is likely to rise on reduction (*65*). Therefore, if a hemoprotein possesses a heme-bound histidine group with the N-1 pK_a in the oxidized state, between, say, 7

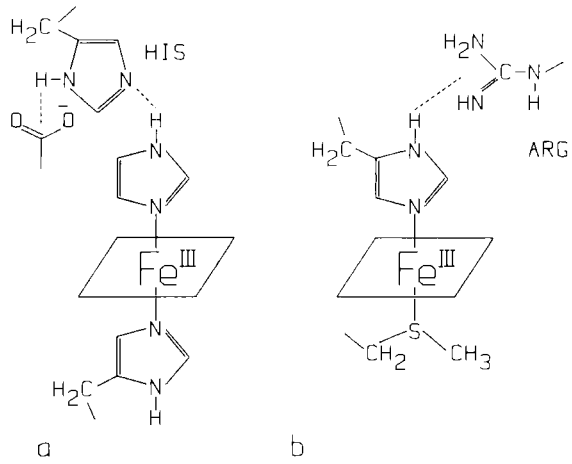

FIG. 13. An illustration of two mechanisms that can promote the loss of the N-3 proton of an imidazole or a histidine ligand bound to low-spin-Fe(III) heme. (a) Imidazole–leghemoglobin *a* (soybean); proton relay via the distal histidine group (*55*). (b) Cytochrome b_{562} (*E. coli*). Arginine 98 has been shown by X-ray crystallography to lie close to the proximal histidine ligand (*53*). The pK_a values of the N-3 proton of the histidine or imidazole ligand in several low-spin Fe(III) hemes are as follows: H_2O, 14.5; metmyoglobin, ~11.0; leghemoglobin, ~7.0; cytochrome b_{562}, 9.0.

and 8, on reduction the pK_a will rise and may lead to reprotonation. This process provides a molecular mechanism for a redox-linked deprotonation–protonation process, one component of a redox proton pump. Redox-driven proton translocation occurs in membrane-spanning proteins such as cytochrome *c* oxidase and ubiquinol oxidoreductases.

2. *Bis(histidine) Ligation with Unusual Orientation*

An unusual cytochrome containing one protoheme IX group in a water-soluble protein (M_r 15,000), designated cytochrome *c″*, has been discovered in the obligate methylotroph, *Methylophilus methylotrophus* (*66*). This hemoprotein is unusual in two respects. First, it is low spin in the ferric state but switches to high spin on one-electron reduction. In the oxidized state the EPR spectrum is dominated by a HALS species with a g_z value of 3.65. This species has a NIR MCD spectrum with E_{CT} of 1560 nm and $\Delta\varepsilon$ of 400 M^{-1} cm^{-1} at 4.2 K and 5 T (Fig. 14) (*67*). This is the intensity predicted for a heme liganded by two histidine groups with their planes oriented close to 90°. The model compound Fe(III)(OEP)(2-methyl-imidazole)$_2$ gives a $\Delta\varepsilon$ value of 370 M^{-1} cm^{-1} and g_z of 3.53 (*61*).

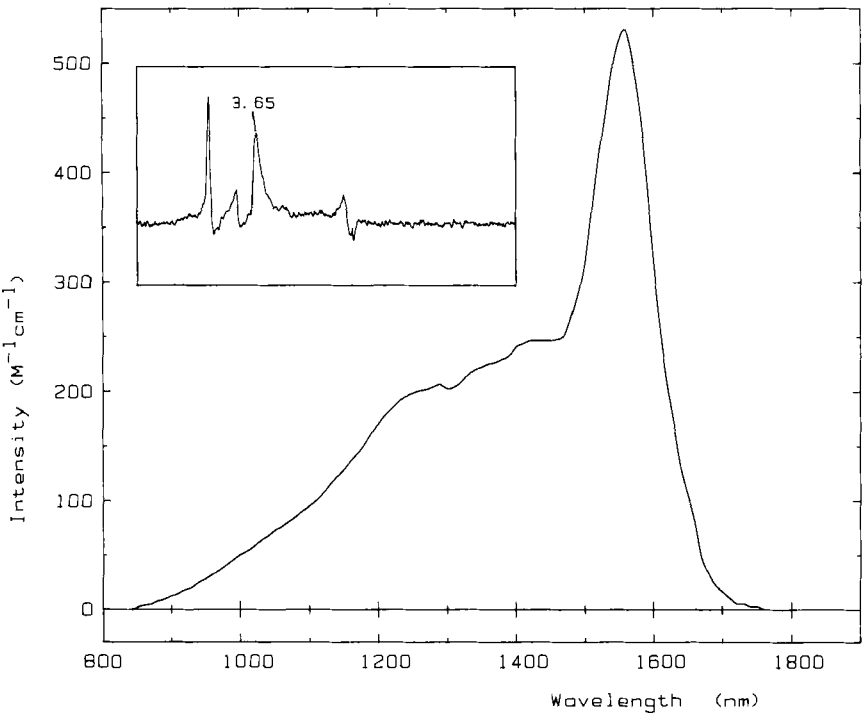

FIG. 14. The NIR MCD spectrum of ferricytochrome *c*″ (*Methylophilus methylotrophus*), measured at 4.2 K and 5 T. The $\Delta\varepsilon$ value of 400 M^{-1} cm^{-1} at 4.2 K and 1.6 K T of the peak at 1560 nm is intense and corresponds to the intensity predicted for bis(histidine) coordination with ring angles close to 90° (*67*). The inset shows the characteristic ramp-shaped g_z component of the EPR spectrum measured at X-band and 5 K.

The membrane-bound cytochrome b_{558} (*Bacillus subtilis*) contains, according to secondary structure predictions, five transmembrane helices. It functions to anchor two other subunits of the succinate quinone oxidoreductase complex (complex II, E.C. 1.3.5.1) in the cytoplasmic membrane (*68*). The 1.3–2.0 hemes per covalently bound flavin have been found with the isolated enzyme. The amino acid residues that bind the heme between the α-helices are likely bis(histidine). The EPR and NIR MCD spectra are consistent with this because the EPR spectra show a g value of 3.4 with a HALS lineshape, and the MCD spectra show a low-spin CT band at 1600 nm with $\Delta\varepsilon$ of 380 M^{-1} cm^{-1} at 4.2 K and 5 T (*69*). This appears to be another example of a bis(histidine)-coordinated heme with near perpendicular alignment of the ligands.

3. *Cytochrome c_4 (Azotobacter vinelandii)*

Cytochrome c_4 contains two heme groups covalently attached to a polypeptide chain (M_r ~20,000). Preliminary X-ray crystallography shows that the irons of the heme are approximately 18 Å apart. Both hemes have similar redox potentials of +263 and +317 mV (*70*). The EPR spectra at 10 K distinguish between the two hemes, which have g_z values of 3.64 and 3.22. The former signal has the characteristic HALS lineshape. The NIR MCD shows a peak at 1900 nm, characteristic of methionine–histidine coordination. Both hemes therefore have the same axial coordination, although one has the HALS EPR signal. One of the heme groups must therefore possess methionine–histidine ligands oriented perpendicular to one another to create a crystal field of low rhombicity (*71*). This example illustrates the importance of having both EPR and NIR MCD evidence for axial ligand assignments.

IV. Heme Peroxidases

A. Introduction

The heme peroxidases catalyze the two-electron oxidation of a substrate by hydrogen peroxide. The substrate is an electron donor such as cytochrome *c* in the case of cytochrome *c* peroxidase (CCP), an organic molecule such as indole acetic acid in the plant enzyme horseradish peroxidase (HRP), and a halide or pseudohalide ion in chloroperoxidase and lactoperoxidase (*72*). Peroxidatic activity is also found in more complex enzymes such as prostaglandin H synthase (PGHS). Catalase, a special case, catalyzes the disproportionation of two molecules of H_2O_2 to H_2O and O_2. The enzymes, which contain a single heme group, must store two oxidizing equivalents after reaction with H_2O_2 (Fig. 15). The ferric form of the heme group reacts with H_2O_2 undergoing one-electron oxidation to the Fe(IV) (d^4) oxidation state, which is stabilized by an oxide ion. This is the so-called ferryl ion, which can be written as $[Fe(II)—O]^{2+}$, $[Fe^{4+}—O^{2-}]^{2+}$, or more usually as $[Fe(IV)=O]^{2+}$. This ion has the ground state $(d_{xy})^2(d_{xz},d_{yz})^2$ with two unpaired electrons giving $S = 1$, which undergoes an axial zero-field splitting of 20–40 cm^{-1}.

The second oxidizing equivalent is removed either from the porphyrin ring or from a protein side chain, depending upon the nature of the enzyme. In the case of HRP (and catalase), the second electron is removed from the porphyrin ring to generate the porphyrin radical cat-

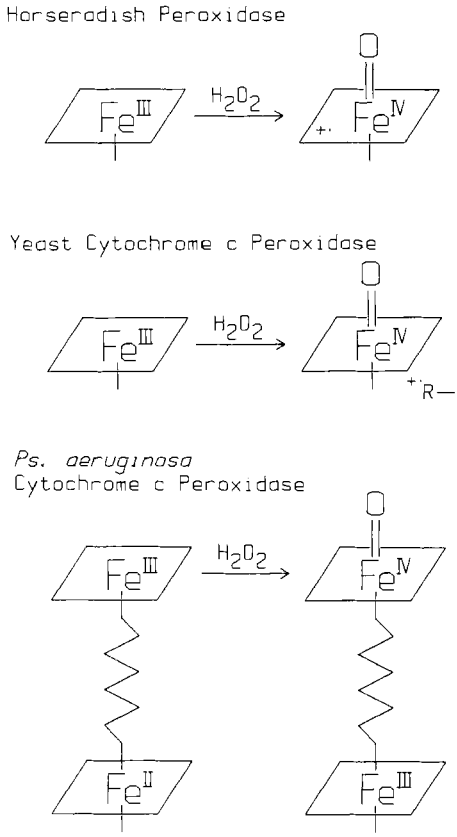

FIG. 15. A schematic diagram illustrating the different two-electron oxidation processes undergone by Fe(III) hemes in horseradish peroxidase [Fe(IV)(por$^{+\cdot}$)], yeast cytochrome *c* peroxidase [Fe(IV(por)(R$^{+\cdot}$)], and diheme cytochrome *c* peroxidase. The porphyrin ring is represented by the square. Histidine is the proximal ligand in all cases. R represents an amino acid side chain.

ion (por$^{+\cdot}$) (*73, 74*). This ensures that both oxidizing equivalents are held at the heme group so that they can be directed toward the oxidation of organic substrates, which become bound within the heme pocket close to the heme edge. In the case of yeast CCP, the second oxidizing equivalent is removed from a protein side chain to generate a radical cation species, —R$^{+\cdot}$, sufficiently remote from the ferryl ion to prevent magnetic interaction with it. There has been long debate about the residue that becomes oxidized to a radical in yeast CCP. Current work using site-directed mutants suggests that a pair of methionine residues are the site of radical trapping.

There is a third class of peroxidases isolable from the bacterial sources such as *P. aeruginosa* and *Pseudomonas stutzerii,* which oxidize cytochrome c_{551}, or azurin. This protein contains two heme protoporphyrin IX groups covalently bound to a single polypeptide side chain. In this enzyme one heme group is oxidized from Fe(III) to Fe(IV)=O and the second heme, from Fe(II) to Fe(III). The oxidizing equivalents are directed to two centers with very different redox potentials (*75*).

The strategy adopted by the monoheme yeast CCP and the bacterial diheme CCP is apparently to distribute the two oxidizing equivalents throughout the protein either on the heme and remote side chain radical or over two heme centers, presumably in order to provide a chain of centers through the enzyme toward the protein partner that provides the reducing equivalents. This contrasts with the peroxidases such as HRP and PGHS, and with catalase, which hold oxidizing equivalents at the heme center so that they are directed at a small organic substrate bound close to the heme, or a second molecule of H_2O_2.

It can be shown that the enzymatic cycle of the diheme CCP involves the oxidation state Fe(III)Fe(IV), in which both heme groups have undergone a one-electron oxidation. However, it has not been demonstrated that in the monoheme CCP from yeast the oxidized protein radical is relevant to the enzymatic cycle. In the absence of substrate, reduced cytochrome *c*, H_2O_2 does indeed oxidize the enzyme to one ferryl ion and one protein-bound radical. However, it is possible that this is a high-energy dead end and that in the presence of excess reduced cytochrome *c* the radical is never produced. Instead the system may operate as a diheme protein, namely, with the protein–protein complex Fe(II)–cytochrome *c*/Fe(III)–CCP undergoing a two-electron oxidation with H_2O_2 to generate Fe(III)–cytochrome *c*/Fe(IV)–CCP. This would be followed by the separation of the two proteins and a further encounter of reduced cytochrome *c* to generate Fe(II)–cytochrome *c*/Fe(IV)–CCP, which finally yields Fe(III)–cytochrome *c* and Fe(III)–CCP.

B. MCD Studies of Ferryl Heme

The two major classes of heme oxidized above the Fe(III) state, namely, the one-electron oxidized ferryl state and the two-electron oxidized state containing Fe(IV)=O and the porphyrin ring cation radical, Fe(IV)(por^{+}), have MCD spectra that provide two useful pieces of information (*76*). First, the form of the spectrum can indicate whether or not the porphyrin ring system is oxidized, and whether the

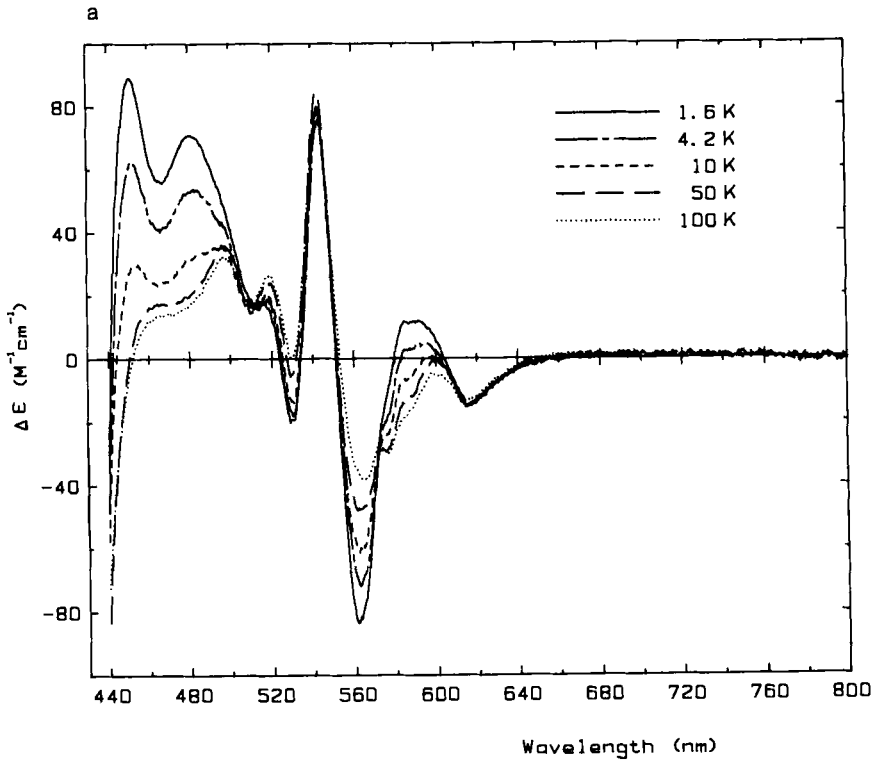
a
80
40
0
-40
-80
ΔE (M⁻¹cm⁻¹)
1.6 K
4.2 K
10 K
50 K
100 K
440
480
520
560
600
640
680
720
760
800
Wavelength (nm)

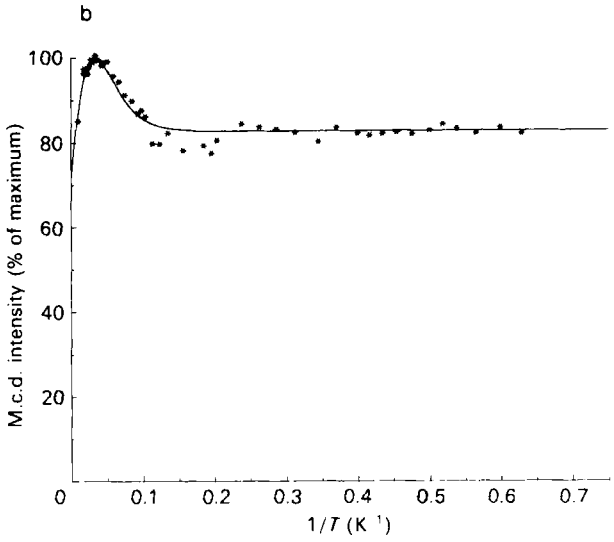
b
100
80
60
40
20
0
M.c.d. intensity (% of maximum)
0.1
0.2
0.3
0.4
0.5
0.6
0.7
1/T (K⁻¹)

ferryl heme is the same species in all cases. Second, the temperature dependence of the MCD spectrum enables the magnetic properties of the electronic ground state to be probed. Because the resulting ferryl ion is an even-spin paramagnet, with $S = 1$, it is EPR silent. Most studies of the magnetic properties of ferryl ion have been carried out with Mössbauer spectroscopy, but this is not ideal for determining parameters of electronic states such as zero-field splitting. We illustrate the use of MCD spectroscopy using examples drawn mainly from our own work.

1. Fe(IV)(por)

Hemoproteins containing the ferryl form of heme, without porphyrin ring oxidation, can be generated in a wide variety of proteins. Reaction of H_2O_2 with deoxymyoglobin leads to a two-electron oxidized state, namely, Fe(IV)–myoglobin, and H_2O_2 reacted with yeast CCP yields a product called compound ES, containing Fe(IV)–heme plus a protein-bound radical. Because the radical contains no optical absorption in the visible region, this is invisible to the MCD spectrum. HRP, on the other hand, can be trapped in a state, called compound II, that contains only the Fe(IV)–heme without the porphyrin radical cation. It is, however, difficult to prepare samples of the ferryl forms that are completely pure and devoid of minor amounts of other oxidation states of heme, especially the Fe(III) oxidation state.

The MCD spectrum at low temperature of the ferryl form of myoglobin is shown in Fig. 16. The temperature dependence, at constant magnetic field, can be fitted to a ground-state spin, $S = 1$, subject to an axial zero-field splitting, D. At very low temperature the MCD spectrum is temperature independent because only the $M_S = 0$ component is populated. On raising the temperature, the $M_S = \pm 1$ levels are populated and the MCD C term intensity grows, leading to an increase in intensity. When kT is greater than D, the Curie law is obeyed and the MCD intensity becomes linearly proportional to $1/T$. By suitable fitting the value of D can be determined. In this way it has been shown that the D values are $28.0 \pm 3\ cm^{-1}$ and $35.0 \pm 5\ cm^{-1}$ for the alkaline and acid forms of ferryl myoglobin (*77*) (see later).

FIG. 16. (a) The MCD spectrum of myoglobin peroxide at pD 3.5, measured at 5 T and several temperatures between 1.6 and 100 K. The spectrum contains two species, Fe(IV) Mb and low-spin Fe(III) Mb, which can be deconvoluted by temperature difference MCD spectroscopy. (b) The temperature dependence of the intensity of the MCD peak at 543 nm of myoglobin peroxide at pD 3.5, and a theoretical curve (——) fitted according to a simple model of the ground state with $S = 1$ and an axial zero-field splitting parameter, $D = 35.0\ cm^{-1}$ (*77*).

The form of the temperature dependence of the $S = 1$ state enables the MCD spectrum of the $S = 1$ form to be separated from that of any contaminating $S = 1/2$ state. The MCD intensity of the latter drops continuously as T is raised, whereas the MCD intensity of the ferryl heme has a maximum in its $1/T$ curve. Hence MCD difference spectra between two temperatures at which the ferryl heme has the same intensity enable the spectrum of the $S = 1/2$ paramagnet to be obtained and thence by back calculation the form of the MCD spectrum of the $S = 1$ form.

In this way a compendium of MCD spectra of the ferryl form of the proteins myoglobin, yeast CCP, and HRP has been compiled (Fig. 17). There is a strong similarity among the spectra of all three, with the exception that ferryl-myoglobin can exist in one of two forms, related by a pK_a process. This was first recognized by Wittenberg (*78*). The low-pH form is similar to that of compound ES, yeast CCP, and compound II HRP. We have suggested that the pK_a process may involve loss of the N-3 proton of the proximal histidine ligand of the heme. It

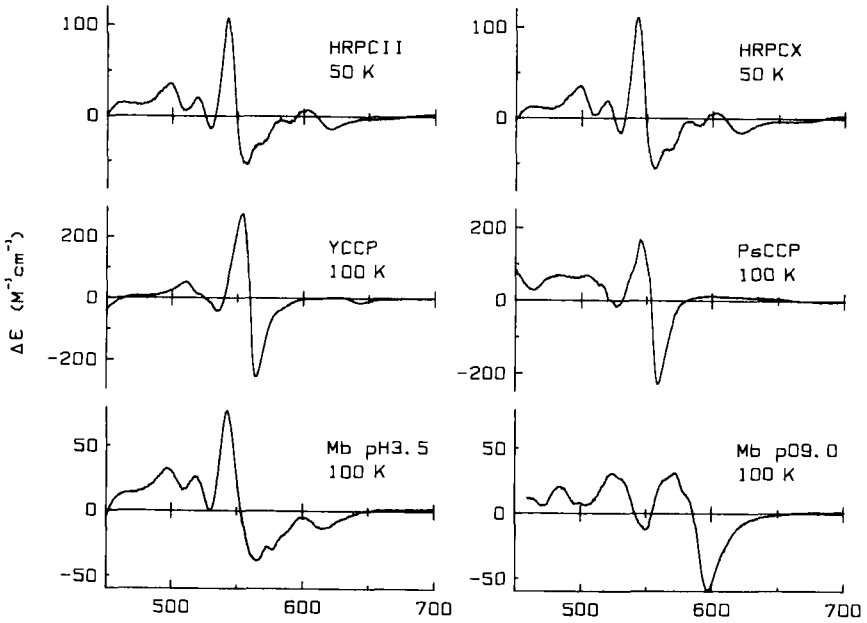

FIG. 17. MCD spectra recorded at 5 T and at 50 or 100 K of Fe(IV)(por) in various protein environments; HRPC II, horseradish peroxidase compound II; HRPCX, horseradish peroxidase compound X; YCCP, yeast cytochrome *c* peroxidase compound ES; PsCCP, compound I of the diheme cytochrome *c* peroxidase; Mb pH 3.5, the ferryl form of myoglobin formed at pH 3.5; Mb pD 9.0, the same compound found at pD 9.0.

seems likely that the ferryl ion, Fe(IV)=O, will be more strongly polarizing than Fe(III) ion and hence may lower the pK_a of N-3 sufficiently for ionization to take place between pH 5–6 (*77*).

2. Fe(IV)(por$^{+\cdot}$)

Oxidation of the porphyrin ring to generate the radical cation, por$^{+\cdot}$, can occur by removal of an electron from either one of the HOMOs $a_{1u}(\pi)$ or $a_{2u}(\pi)$. This results in a major perturbation of the optical spectrum of the porphyrin ring (*73*). The detailed assignments of the new feature are uncertain. This radical species can be generated either chemically or electrochemically by one-electron oxidation of metal-free porphyrin.

Oxidation of a metal-containing porphyrin results in ring oxidation only if the metal ion is either redox inactive, such as Zn(II) or Mg(II), or difficult to oxidize further, such as Co(III). In the case of the heme ring one-electron, oxidation invariably leads to metal ion oxidation to the Fe(IV) state. There are two reported instances in which the ring alone can be oxidized to generate Fe(III)(por$^{+\cdot}$), but this requires an axial ligand such as Cl^- or perchlorate (*79, 80*). There is no well-substantiated report of ring-only oxidation taking place in a protein-bound heme, although the presence of OH^- as a ligand to Fe(III) should favor the oxidation of the ring alone. We have suggested that addition of a proton to compound II of HRP might favor a shift of the oxidizing equivalent from Fe(IV) to the porphyrin ring (*76*), thus

$$\text{Fe(IV)=O(por)} \xrightarrow{H^+} \text{Fe(IV)—OH}^+\text{(por)} \rightarrow \text{Fe(III)—OH(por}^{+\cdot}\text{)}$$

This would have the advantage of moving oxidizing equivalents toward the periphery of the porphyrin ring close to the substrate that is to be oxidized. However, we have been unable to identify this species with certainty (*76, 81*).

The two-electron oxidized form of the heme ring in HRP corresponds to Fe(IV)=O(por$^{+\cdot}$). The two unpaired electrons of Fe(IV) ($S = 1$) couple to the single unpaired electron of (por$^{+\cdot}$) ($S = 1/2$) to give overall spin states $S = 3/2$ and $S = 1/2$ (*82*). The MCD spectrum of this form of HRP, compound I, shows the grossly modified form of the porphyrin spectrum and the strong temperature dependence of the paramagnetic ground state (Fig. 18). The magnetization curves at 1.6 K prove that the lowest state is a doublet with $S = 1/2$. In principle, the higher excited state $S = 3/2$ could be located by a study of the temperature dependence of the MCD spectrum (*83*). This has not been attempted.

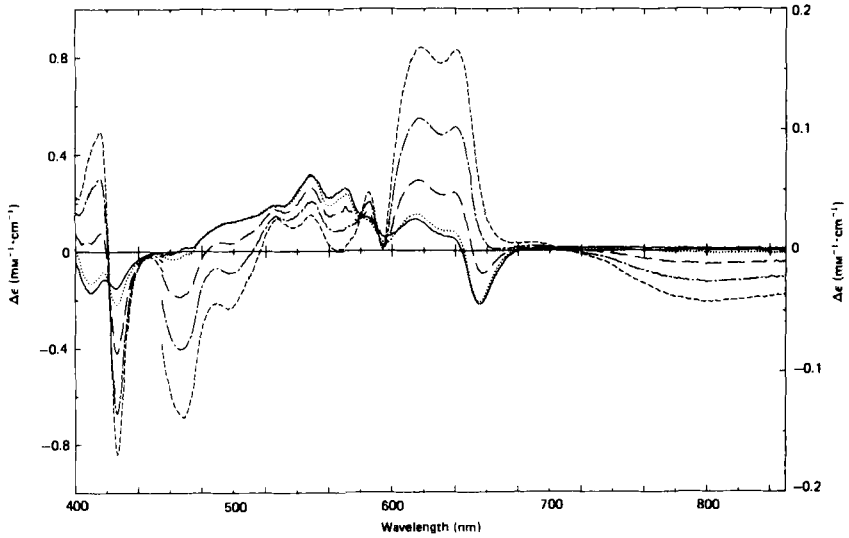

FIG. 18. The MCD spectrum of horseradish peroxidase compound I, recorded at 5 T and several temperatures between 1.6 and 75 K. The species consists of Fe(IV)(por$^{+\cdot}$).

C. DIHEME CYTOCHROME *c* PEROXIDASE (*Pseudomonas aeruginosa*)

Cytochrome c_{551} peroxidase (E.C. 1.11.1.5) catalyzes the oxidation of 2 mol of ferrocytochrome c_{551} by hydrogen peroxide. The enzyme differs from other peroxidases in having two heme *c* moieties covalently attached to a single polypeptide chain. The $E_{7,m}$ values of the two hemes are +320 and −330 mV, respectively (*84*). The enzyme in the fully oxidized state is unreactive toward H_2O_2. Reduction of the high-potential heme is required before reaction with H_2O_2 can take place. NIR MCD spectra of the fully oxidized and half-reduced forms of the enzyme at room temperature and 4.2 K enabled the heme axial ligands and spin states to be identified (Fig. 19). At room temperature in the oxidized state, the low-potential heme is low spin and coordinated by two histidine ligands (*85*). Although the high-potential heme has histidine–methionine ligation, the heme appears to be in a high/low-spin thermal equilibrium. At 4.2 K the heme is fully low spin (*86*). There is evidence that in several cytochromes of the *c* type that are low spin at room temperature, the high-spin excited state is thermally accessible at ~60°C. In the diheme peroxidase the high-spin state is partially populated at room temperature. This may result from heme–heme interaction (*87*).

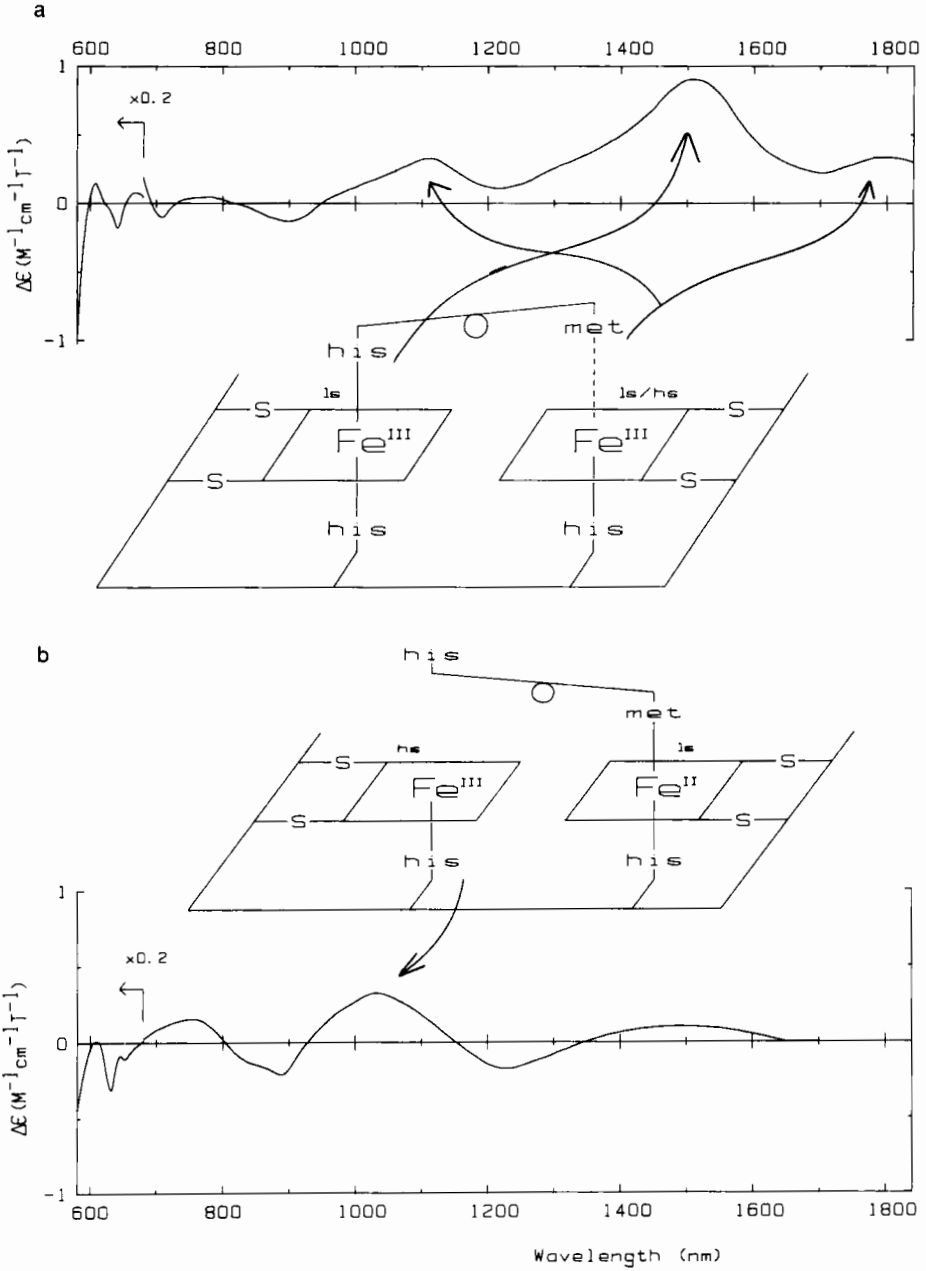

FIG. 19. The NIR MCD spectra at room temperature of (a) oxidized and (b) semireduced diheme cytochrome *c* peroxidase (*Pseudomonas aeruginosa*). The assignments of the various features of the spectra are indicated in terms of a simple model of heme ligation. (c) The complete enzymatic cycle established by MCD and EPR spectroscopy in terms of the oxidation levels of the two hemes.

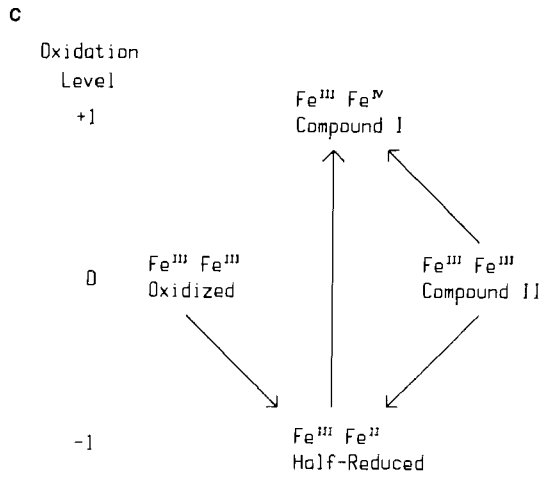

FIG. 19. (*continued*)

The addition of one electron to the high-potential heme causes it to become fully low-spin ferrous and induces the high-potential heme to change its spin state from low to high by the loss of an axial histidine ligand. This ensures that a typical peroxidatic heme center, coordinated by a proximal histidine ligand with an uncoordinated histidine group present in the distal pocket, is generated *only* after addition of one electron to the enzyme. The half-reduced state of the enzyme reacts rapidly with H_2O_2, undergoing oxidation of the low-potential heme to the ferryl form and the high-potential heme to the Fe(III) state. The presence of low-spin Fe(III) heme is evidenced by the NIR MCD spectrum, although peak wavelength of the CT band at 1720 nm is unusually short for methionine–histidine coordination. The presence of a "695"-nm band is good evidence for this axial ligation. The ferryl heme is confirmed by the identification at 100 K of the appropriate MCD signature (see Fig. 17). The complete catalytic cycle is shown in Fig. 19c (*75*).

There is ample of evidence for the presence of heme–heme interaction in this enzyme. Proteolysis of the enzyme leads to the loss of a small polypeptide fragment, abolishes the activity of the enzyme, and prevents the low-potential heme from switching to high spin on reduction of the high-potential heme. The mechanism of the axial ligand loss in the active enzyme, which is induced by reduction of the other heme, also points to the cooperative nature of the protein. The spectroscopic parameters of one heme, such as the value of E_{CT}, depend upon the oxidation state of the other heme. The form of the enzyme possessing

two Fe(III) hemes generated by catalytic turnover is unlike the resting state of the protein. The mechanism of this heme–heme interaction is obscure because the structure of the protein is not known, but it is likely that the interaction is mediated by the protein structure, rather than the proximity of the two hemes.

V. Metal Centers of Cytochrome *c* Oxidase

A. Introduction

Cytochrome *c* oxidase catalyzes the transfer of four electrons and four protons to dioxygen to generate 2 mol of water in the terminal act of aerobic respiration carried out by the mitochondrion (*88*). The enzyme spans the mitochondrial inner membrane and pumps protons from inside to the outside to generate a proton gradient that is subsequently used to drive the condensation of ADP and phosphate to yield ATP. Mammalian cytochrome *c* oxidase is a protein of great complexity, consisting of at least 12 subunits. However, the same essential reactions involving dioxygen reduction and proton pumping are carried out by bacterial oxidases, exemplified by cytochrome *c* oxidase from *Paracoccus denitrificans* (*89*). This enzyme contains only three subunits (*90*, *91*).

The redox chemistry is carried out by the highly cooperative activity of four metal centers involving two heme groups, of the *a* type, and at least two containing copper. The total number of copper ions per mole of enzyme is the subject of dispute currently, but the evidence from careful analytical results shows the presence of three copper ions (*92*). In addition, the presence of zinc has been reported (*93*). Three of the metal centers are found in one polypeptide, subunit I. They are cytochrome *a*, a heme center liganded by two histidine residues, which remains low spin throughout the redox cycle, and cytochrome a_3, which is close to one of the copper centers, called Cu_B. This pair of centers is involved in dioxygen binding and reduction. The other copper center, called Cu_A, bound to subunit II, is likely the site of electron entry from reduced cytochrome *c* and is probably located at the surface of the membrane (*94*). The structure of the Cu_A center is the subject of discussion. It has long been supposed that this center contains a single copper ion liganded by two histidine and two cysteine residues (*95*). However, there is new evidence emerging that suggests the site may consist of a pair of interacting copper ions that undergo a one-electron redox cycle from the mixed-valence Cu(I)/Cu(II) state to the Cu(I)/

Cu(I) state. It has been proposed that a site of similar structure is present in the enzyme nitrous oxide reductase (*96, 97*).

Recent advances in cloning and sequencing two bacterial oxidases, ubiquinol oxidoreductase, show over 80% homology between the sequence of subunit I of aa_3 and ubiquinol oxidoreductase from *E. coli* (*98*). The latter enzyme reduces dioxygen to water using four reducing equivalents obtained from reduced ubiquinol that is located in the membrane. There appears to be a good deal of structural homology between these two enzymes. Ubiquinol oxidoreductase contains two heme centers, called cytochrome *b* and cytochrome *o*, and one copper ion. This enzyme is also transmembrane spanning but lacks subunit II and the Cu_A center. The structural parallels between aa_3 and *bo* and recent EPR redox titrations suggest the presence of a heme–Cu_B pair capable of reducing dioxygen in both enzymes (*99*).

B. MCD Studies of Cytochrome *c* Oxidase

Cytochrome *c* oxidase contains four metal centers of different optical and magnetic characteristics. The deconvolution of the properties of each one has proved problematical and controversial. However, MCD spectroscopy is ideally suited to the study of such complex metalloproteins because it has a selectivity for individual metal centers based upon the magnetization properties of each and also because there is better energy resolution of metal centers in the NIR wavelength region. In many chromophores the density of electronic states increases to higher energy and vice versa. This gives the opportunity to resolve the optical bands due to individual metal centers by measuring the electronic spectrum in the NIR.

Our study of bovine cytochrome *c* oxidase illustrates these principles (*13, 14*). The oxidized enzyme shows in the EPR spectrum two paramagnetic species, low-spin Fe(III) cytochrome *a* (g = 3.03, 2.21, and 1.50), and one spin assigned to Cu_A (g = 2.18, 2.03, and 1.98). There are other minor signals whose intensity depends on the enzyme preparation and the previous history of the sample. The oxidized state of the enzyme will bind 1 mol of cyanide ion, but the EPR spectrum is unchanged, with only two paramagnetic centers, each possessing one spin per mole of enzyme, being detectable. The NIR MCD spectrum of the oxidized and the oxidized cyanide-inhibited form of the enzyme is very revealing (Fig. 20). The MCD magnetization properties of each one of the major peaks or troughs in the spectrum were measured and are compared in Fig. 21 by normalizing to the same absolute intensity at 1.6 K and the 5-T field. It is clear that the trough at 790 nm and the

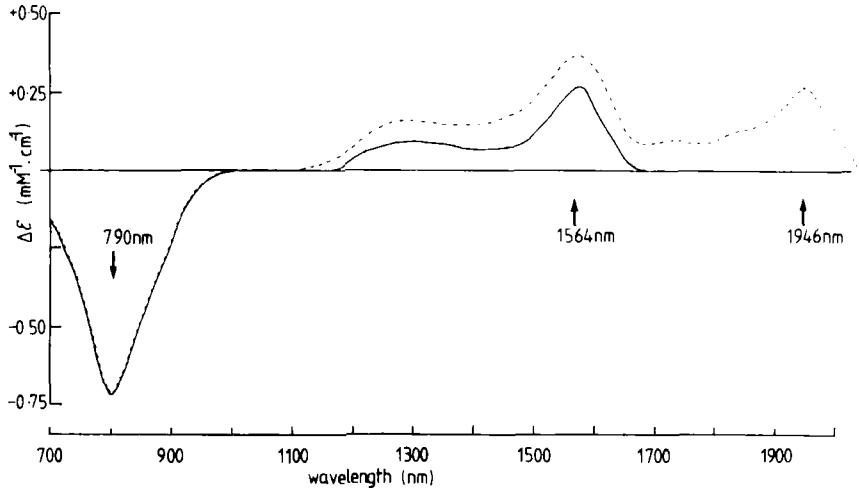

FIG. 20. The NIR MCD spectra of oxidized bovine cytochrome *c* oxidase with (dashed line) and without (solid line) CN^- binding. The spectra are recorded at 4.2 K and 5 T. Arrows indicate the wavelengths at which MCD magnetization curves were measured (see Fig. 21).

peaks at 1560 and 1946 nm have different initial slopes in the magnetization curves, showing that these three bands arise from three different paramagnetic species. Indeed, the magnetization curve of the trough at 790 nm can be fitted to a spin $S = 1/2$ paramagnet with the g values of ~2.0, implying that this MCD feature must belong to the EPR-detectable center called Cu_A. The peak at 1560 nm magnetizes with curves that can be fitted with the g values of cytochrome *a*. This band has the form of a low-spin ferric heme and with a wavelength consistent with coordination by a pair of histidine ligands. This early established the coordination of cytochrome *a* (*100*). However, the most interesting feature of the NIR MCD spectra is the peak at 1946 nm, which is found *only* in the cyanide-inhibited form of the bovine enzyme. The magnetization curves imply that this band arises from a paramagnetic species with a ground-state electronic doublet. But because this peak magnetizes differently from the other two and no other major EPR signals are found, we can conclude that the 1946-nm band represents an EPR-silent paramagnet. Furthermore, this band is induced to appear by the binding of CN^- ion to cytochrome a_3. The form of the spectrum is that of a low-spin Fe(III) heme CT band. Therefore, this is an optical band characteristic of cyanide-bound cytochrome a_3. It is known from experiments on the reduced state of the enzyme that cytochrome a_3 has one histidine group as the proximal ligand (*101*).

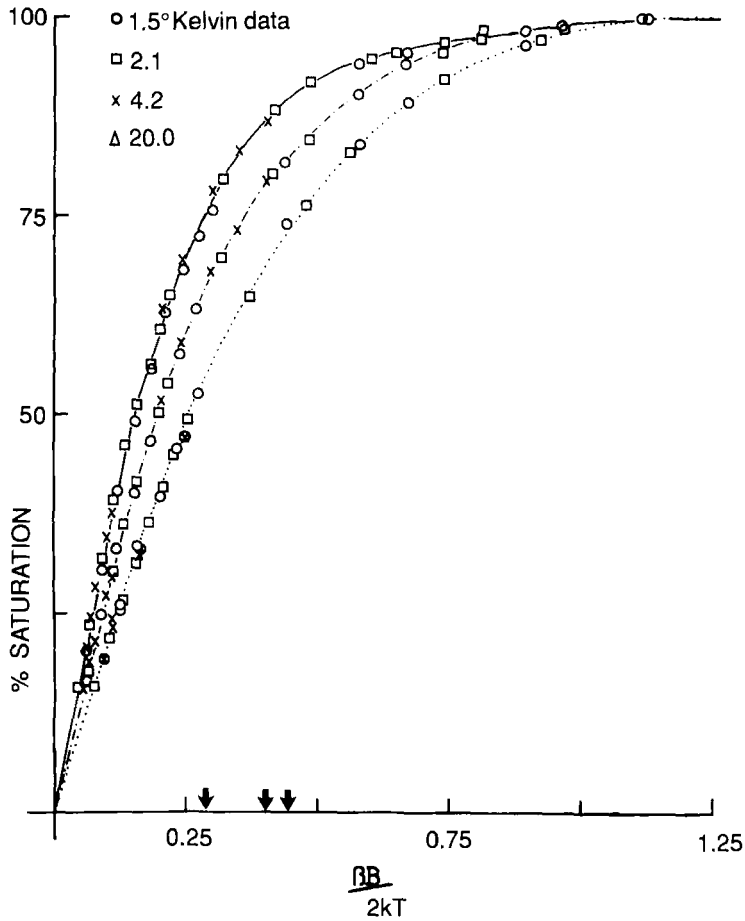

FIG. 21. The MCD magnetization curves of the bands at 790, 1564, and 1946 nm in the NIR MCD spectra of oxidized cytochrome *c* oxidase and its cyanide-inhibited state (see Fig. 20). The saturation magnetization intensities are normalized to 100. The *I* values calculated for $g = 2.0$, $g = 3.03$, 2.22, and 1.50, and $g_{\parallel} = 5.6 \pm 0.4$, $g_{\perp} = 0$ are shown on the abscissa. These correspond to $Cu_A(II)$, ferricytochrome *a*, and the cytochrome a_3–$Cu_B(II)$ pair bridged by CN^-, respectively.

The NIR CT band for the CN^-/histidine-ligated heme should occur at a wavelength of ~1600 nm (*52*). The CT band in CN/aa_3 has shifted to 1946 nm.

These facts about the cytochrome a_3 site, inhibited by CN^-, can be interpreted in the following way. Cytochrome a_3 is EPR silent but has a ground state with an electronic doublet as the lowest energy compo-

nent. Careful experiments measuring the temperature dependence of the MCD intensity reveal the presence of a further component of the ground state between 10 and 20 cm^{-1} above the ground state (*13*). These results point to a ground state of $S = 1$, subject to a large axial zero-field splitting, D, between -10 and -20 cm^{-1}. The MCD magnetization properties at 1.6 K give, via the intercept value, effective g values of $g_{\|} = 5.6 \pm 0.4$, assuming $g_{\perp} = 0$. These magnetic properties can arise only by the *ferromagnetic* coupling of $S_1 = 1/2$, from low-spin cyanide-bound cytochrome a_3, with $S_2 = 1/2$ on Cu_B(II). Low-spin heme bound by CN^-, such as metMbCN, and partially reduced cytochrome c oxidase that is CN^- bound give g_z values of 3.45 and 3.58, respectively. Assuming that Cu_B^{2+} has a g value of ~2.0 in the direction parallel to the heme g_z value, the resulting effective g value along the direction normal to the heme plane is predicted to be $3.5 + 2.0 \approx 5.5$, well within the experimental value of 5.6 ± 0.4 determined from MCD magnetization (*14*).

The CN^- group must mediate the ferromagnetic interaction between a_3 and Cu_B. As an ambidentate ligand it can bridge the two centers. This may account also for the unexpectedly long wavelength of the a_3 NIR CT band because the axial ligand to a_3 is not CN^-, but rather $C{\equiv}N{-}Cu_B^{2+}$. This view is confirmed by experiments that show that NO can bind to oxidized Cu_B^{2+} without breaking the CN^- bridge (*102*). The NIR CT band shifts from 1946 to 1785 nm. Hence binding NO to Cu_B^{2+} shifts the *heme* CT band. The interaction is transmitted via the CN^- bridge. On reduction of Cu_B^{2+} with dithionite, the bridge is broken and the cyanide-bound cytochrome a_3 becomes EPR detectable, with a g_z of 3.58, and the NIR CT band shifts from 1946 to 1550 nm, the wavelength expected for an isolated CN^--bound heme (*103*).

The remaining question concerns the nature of the coupling between a_3 and Cu_B that gives rise to a ferromagnetic coupling. It is well known that ferromagnetic exchange between two metal centers in a dimer requires an orthogonal exchange pathway. This is an expression of the Hund spin-pairing rule that unpaired electrons in orthogonal orbitals with parallel spins will be a lower energy configuration than will those with paired spins. Overlap exchange leads to the pairing of spins because it corresponds to incipient bond formation. Hence, in the exchange pathway from Fe(III) to Cu(II) there must be an odd number of orthogonal overlaps. Figure 22 suggests one possible solution to this problem. The unpaired electron on the Fe(III) ion is located partially in the d_{xz} and d_{yz} orbitals. The orientation of the orbital containing the unpaired electron on Cu_B^{2+} is not known. One possibility is indicated. The requirement for an orthogonal step in the pathway to bring about

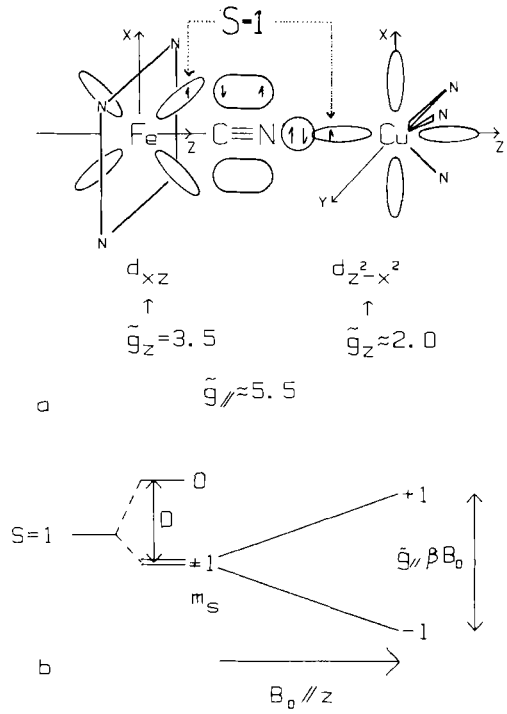

FIG. 22. (a) An orbital pathway capable of promoting ferromagnetic exchange between a single d electron of low-spin Fe(III) heme a_3 and of Cu_B(II) when mediated by a bridging CN^- group. Note that the Fe—C≡N—Cu atoms must be closely colinear in order for ferromagnetic exchange to dominate antiferromagnetic exchange pathways. Orbitals that overlap cause electrons to pair, whereas orthogonal orbitals maintain electrons parallel. The predicted value of $g_{\parallel}$ of the coupled system is given by the sum of the g value components of Fe(III) and Cu(II) along the line joining the two ions. (b) The energy levels of the ferromagnetically coupled bridge Fe(III)—C≡N—Cu(II) as determined from MCD magnetization properties. The ground-state total spin $S = 1$ ($S_1 = S_2 = 1/2$) is split by a strong axial distortion D of negative sign, estimated at between -10 and -20 cm^{-1}. The rhombic splitting of $M_S = \pm 1$ is less than 1 cm^{-1}. EPR transitions within the ground-state doublet are forbidden.

ferromagnetic exchange necessitates a linear arrangement of the four atoms Fe(III)—C≡N—Cu(II). Departure from linearity will introduce overlap exchange pathways, which bring about antiferromagnetic contributions of greater magnitude than ferromagnetic exchange and hence invariably overwhelm the latter. Thus the structural requirements to promote ferromagnetic exchange are rather strict and, in our view, testify to the high degree of linearity of the bridge, Fe—C≡N—Cu.

The fact that the anion $C{\equiv}N^-$ can bridge the Fe(III) of a_3 and Cu(II) of the Cu_B center in a linear fashion may bear upon the way in which dioxygen binds to the reduced state of the enzyme. Cyanide is a competitive inhibitor of dioxygen binding to the reduced state of the enzyme. The bond length of O_2 is 1.21 Å compared with 1.15 Å for the $C{\equiv}N^-$. Hence it is reasonable to propose that in the reduced state of the enzyme, dioxygen can bridge, in a linear fashion, between a_3 and Cu_B, thus, Fe(II)—O=O—Cu_B(I). The reductive cleavage of dioxygen, which is bound linearly between two metal ions, poses interesting steric questions. Electron transfer toward dioxygen will result in the formation of Fe(III)—O^{2-}—O—Cu(II), at which stage the dioxygen bond is at its weakest. Before protons or further electrons can be introduced, the O—O bond must be broken. There is evidence that the act of transferring further electrons into the a_3/Cu_B site from cytochrome a and, perhaps, Cu_A, causes a conformational change in the enzyme (*104*). If this were such as to move Fe(III) and Cu_B(II) further apart, this would assist in breaking the peroxide ion bond.

A comparative study of the metal centers in cytochrome c oxidase from several bacterial sources, including *Thermus thermophilus* and *P. denitrificans,* using EPR and MCD spectroscopy has established that in both cases cytochrome a is liganded by two histidine oxidases and the Cu_A^{2+} center is identical to that in bovine cytochrome c oxidase (*105, 106*). The properties of the cytochrome a_3/Cu_B dimer have not been established to be identical, although ferrocytochrome a_3 is high-spin ferrous, as expected. Recent studies of the MCD properties of the Cu_A^{2+} center in cytochrome c oxidase and a copper center in nitrous oxide reductase (*107, 108*) show that the two centers are virtually identical. The evidence from the EPR hyperfine structure of the copper center in nitrous oxide reductase suggests that the center in this enzyme is a mixed-valence Cu(I)/Cu(II) dimer, which raises the interesting prospect that the Cu_A center in cytochrome c oxidase is also a dimeric copper species.

ACKNOWLEDGMENTS

Much of the work reviewed here has been carried out by former students and postdoctoral fellows, including D. G. Eglinton, M. K. Johnson, P. M. A. Gadsby, N. Foote, D. Barber, J. Peterson, P. E. Gooding, J. P. Springall, C. P. Barrett, B. C. Hill, T. C. Woon, and T. Brittain. We have also received supplies of protein samples from G. Sievers, C. A. Appleby, H. Santos, D. L. Turner, P. M. Harrison, J. Reichardt, L. Hederstedt, G. R. Moore, F. Kadir, R. K. Thauer, and D. Ankel-Fuchs. Our work has been generously and continuously supported by the SERC, especially the Molecular Recognition Initia-

tive, under whose auspices the UEA group has been designated a Centre of Metalloprotein Spectroscopy and Biology. The Royal Society, The Wellcome Trust, The Petroleum Research Fund, and NATO have also provided support.

We have benefited from discussions with G. R. Moore, R. Grinter, P. Nicholls, M. J. Stillman, C. A. Reed, P. J. Stephens, and A. Walker.

References

1. MacMunn, C. A., *Philos. Trans. R. Soc. London* **177,** 267 (1886).
2. Keilin, D., *in* "The History of Cell Respiration and Cytochromes" (J. Keilin, ed.) Cambridge Univ. Press, Cambridge, 1966.
3. Williams, R. J. P., *Chem. Rev.* **5,** 299 (1956).
4. Shashoua, V. E., *J. Am. Chem. Soc.* **882,** 5505 (1960); *Nature (London)* **203,** 972 (1964); *J. Am. Chem. Soc.* **87,** 4044 (1965).
5. Stephens, P. J., Ph.D. Thesis, Oxford University (1964).
6. Stephens, P. J., Suetaka, W., and Schatz, P. N., *J. Chem. Phys.* **44,** 4592 (1966).
7. Dratz, E. A., Ph.D. Thesis, University of California, Berkeley (1966).
8. Vickery, L., Nozawa, T., and Sauer, K., *J. Am. Chem. Soc.* **98,** 343 (1976).
9. Briat, B., Berger, D., and Leliboux, M., *J. Chem. Phys.* **57,** 5606 (1972).
10. Thomson, A. J., and Johnson, M. K., *Biochem. J.* **191,** 411 (1980).
11. Cheng, J. C., Osborne, G. A., Stephens, P. J., and Eaton, W. A., *Nature (London)* **241,** 193 (1973).
12. Greenwood, C., and Wilson, M., *Eur. J. Biochem.* **22,** 5 (1971).
13. Thomson, A. J., Johnson, M. K., Greenwood, C., and Gooding, P. E., *Biochem. J.* **193,** 687 (1981).
14. Thomson, A. J., Eglinton, D. G., Hill, B. C., and Greenwood, C., *Biochem. J.* **207,** 167 (1982).
15. Barrett, C. P., Peterson, J., Greenwood, C., and Thomson, A. J., *J. Am. Chem. Soc.* **108,** 3170 (1986).
16. Barnes, J. C., and Thomson, A. J., *J. Sci. Instrum.* **44,** 577 (1967).
17. Day, P., Smith, D. W., and Williams, R. J. P., *Biochemistry* **6,** 1563, 3747 (1967).
18. Schatz, P. N., and McCaffery, A. J., *Q. Rev., Chem. Soc.* **23,** 552(1969); **24,** 329 (1970).
19. Stephens, P. J., *Adv. Chem. Phys.* **35,** 197 (1976).
20. Piepho, S. B., and Schatz, P. N., "Group Theory in Spectroscopy, with Applications to Magnetic Circular Dichroism." Wiley, New York, 1983.
21. Goutermann, M., and Wagnière, G. H., *J. Mol. Spectrosc.* 11, 108 (1963).
22. Simpson, W. T., *J. Chem. Phys.* **17,** 1218 (1949).
23. Keegan, J. D., Stolzenberg, A. M., Lu, Y.-C., Linder, R. E., Barth, G., Bunnenberg, E., and Djerassai, C., *J. Am. Chem. Soc.* **103,** 3201 (1981).
24. Briat, B., Schooley, D. A., Records, R., Bunnenberg, E., and Djerassi, C., *J. Am. Chem. Soc.* **89,** 6170 (1967).
25. Smith, D. W., and Williams, R. J. P., *Struct. Bonding (Berlin)* **6,** 3747 (1967).
26. Cheesman, M. R., Ankel-Fuchs, D., Thauer, R. K., and Thomson, A. J., *Biochem. J.* **260,** 613 (1989).
27. Misiura, A. J., Ph.D. Thesis, University of East Anglia, Norwich, England (1989).
28. Gale, R., McCaffery, A. J., and Rowe, M. D., *J. Chem. Soc., Dalton Trans.* 596 (1972).

29. Browett, W. R., Fucaloro, A. F., Morgan, T. V., and Stephens, P. J., *J. Am. Chem. Soc.* **105,** 1868 (1983).
30. Sutherland, J. C., and Klein, M. P., *J. Chem. Phys.* **57,** 76 (1972).
31. McHugh, A. J., and Goutermann, M., *Theor. Chim. Acta* **24,** 346 (1972).
32. Gadsby, P. M. A., Ph.D. Thesis, University of East Anglia, Norwich, England (1984).
33. Eaton, W. A., and Charney, E., *J. Chem. Phys.* **51,** 4502 (1969).
34. Huynh, B. H., Papaefthymiou, G. C., Yen, C. S., Groves, J. L., and Wu, C. S., *J. Chem. Phys.* **61,** 3750 (1974).
35. Eglinton, D. G., Johnson, M. K., Thomson, A. J., Gooding, P. E., and Greenwood, C., *Biochem. J.* **191,** 319 (1980).
36. Eaton, W. A., Hanson, L. K., Stephens, P. J., Sutherland, J. C., and Dunn, J. B. R., *J. Am. Chem. Soc.* **100,** 4991 (1978).
37. Nakons, N., Otsuka, J., and Tasaki, A., *Biochim. Biophys. Acta* **236,** 222 (1971).
38. Brittain, T., Greenwood, C., Springall, J. P., and Thomson, A. J., *Biochim. Biophys. Acta* **703,** 117 (1982).
39. Sharanov, Y. A., Sharanova, N. A., Figlovsky, V. A., and Grigorjev, V. A., *Biochim. Biophys. Acta* **709,** 332 (1982).
40. Makinen, M. W., and Churg, A. K., *in* "Iron Porphyrins" (A. B. P. Lever and H. B. Gray, eds.), Part I, pp. 141–230. Addison-Wesley, Reading, Massachusetts, 1983.
41. Gibson, Q. H., *Biochem. J.* **71,** 293 (1959).
42. Eaton, W. A., and Hochstrasser, R. M., *J. Chem. Phys.* **46,** 2533 (1967).
43. Braterman, P. S., Davies, R. C., and Williams, R. J. P., *Adv. Chem. Phys.* 7, 359 (1964).
44. Stephens, P. J., Sutherland, J. C., Cheng, J. C., and Eaton, W. A., *in* "Excited States of Biological Molecular Processes" (J. B. Birks, ed.), p. 434. Wiley, Chichester, 1976.
45. Rots, M. I. F., and Zandstra, P. J., *Mol. Phys.* **46,** 1283 (1982).
46. English, D. R., Hendrickson, D. N., Suslick, K. S., Eiogenbrot, C. W., and Scheidt, W. R., *J. Am. Chem. Soc.* **106,** 7258 (1984).
47. Blumberg, W. E., and Peisach, J., *in* "Probes of Structure and Function of Macromolecules and Membranes" (B. Chance, T. Yonetani, and A. S. Mildvan, eds.), Vol. 2, pp. 215–229. Academic Press, New York, 1971.
48. Gadsby, P. M. A., and Thomson, A. J., *J. Am. Chem. Soc.* **112,** 5003 (1990).
49. Nafie, L. A., Keiderling, T. A., and Stephens, P. J., *J. Am. Chem. Soc.* **98,** 2715 (1976).
50. Thomson, A. J., and Gadsby, P. M. A., *J. Chem. Soc., Dalton Trans.* 1921 (1990).
51. Eglinton, D. G., Gadsby, P. M. A., Sievers, G., Peterson, J., and Thomson, A. J., *Biochim. Biophys. Acta* **742,** 648 (1983).
52. Cheesman, M. R., McKnight, J., Reed, C. A., and Thomson, A. J., *Inorg. Chem.* (submitted for publication).
53. Moore, G. R., Williams, R. J. P., Peterson, J., Thomson, A. J., and Mathews, F. S., *Biochim. Biophys. Acta* **829,** 83 (1985).
54. Gadsby, P. M. A., and Thomson, A. J., *FEBS Lett.* **150,** 59 (1982).
55. Sievers, G., Gadsby, P. M. A., Peterson, J., and Thomson, A. J., *Biochim. Biophys. Acta* **742,** 637 (1983).
56. Rigby, S. E. J., Moore, G. R., Gray, J. C., Gadsby, P. M. A., George, S. J., and Thomson, A. J., *Biochem. J.* **256,** 571 (1988).
57. Gadsby, P. M. A., Peterson, J., Foote, N., Greenwood, C., and Thomson, A. J., *Biochem. J.* **246,** 43 (1987).

58. Cheesman, M. R., Kadir, F., Moore, G. R., Greenwood, C., and Thomson, A. J., *Nature (London)* **346,** 771 (1990).
59. Thomson, A. J., and Gadsby, P. M. A., *J. Chem. Soc., Dalton Trans.* 1921 (1990).
60. Salerno, J. C., *J. Biol. Chem.* **259,** 2331 (1984).
61. Gadsby, P. M. A., and Thomson, A. J., *FEBS Lett.* **197,** 253 (1986).
62. Scheidt, W. R., Kirner, J. F., Hoard, J. E., and Reed, C. A., *J. Am. Chem. Soc.* **109,** 1963 (1987).
63. Rawlings, J., Stephens, P. J., Nafie, L. A., and Kamen, M. D., *Biochemistry* **16,** 1726 (1977).
64. Maltempo, M. M., and Moss, T. H., *Q. Rev. Biophys.* **9,** 181 (1976).
65. de Ropp, J. S., Thanabal, V., and La Mar, G. N., *J. Am. Chem. Soc.* **107,** 8268 (1985).
66. Santos, H., and Turner, D. L., *Biochim. Biophys. Acta* **954,** 237 (1988).
67. Berry, M. J., George, S. J., Thomson, A. J., Santos, H., and Turner, D. L., *Biochem. J.* **270,** 413 (1990).
68. Hederstedt, L., *in* "Methods in Enzymology" (S. Fleischer and B. Fleischer, eds.), Vol. 126, p. 339. Academic Press, Orlando, Florida, 1986.
69. Friden, H., Cheesman, M. R., Hederstedt, L., Andersson, K. K., and Thomson, A. J., *Biochim. Biophys. Acta* **1041,** 207 (1990).
70. Ambler, R. P., Daniel, M., Melis, K., and Stout, C. D., *Biochem. J.* **222,** 217 (1984).
71. Gadsby, P. M. A., Hartshorn, R. T., Moura, J. J. G., Sinclair-Day, J. D., Sykes, A. G., and Thomson, A. J., *Biochim. Biophys. Acta* **994,** 37 (1989).
72. Dunford, H. B., and Stillman, J. S., *Coord. Chem. Rev.* **19,** 187 (1976).
73. Dolphin, D., Forman, A., Borg, D. C., Fajer, J., and Felton, R. H., *Proc. Natl. Acad. Sci. U.S.A.* **68,** 614 (1971).
74. Roberts, J. E., Hoffmann, B. M., Ruther, R., and Hager, L. P., *J. Biol. Chem.* **256,** 2118 (1981).
75. Greenwood, C., Foote, N., Gadsby, P. M. A., and Thomson, A. J., *Chem. Scr.* **28A,** 79 (1988).
76. Thomson, A. J., Greenwood, C., Gadsby, P. M. A., and Foote, N., *in* "Cytochrome Systems: Molecular Biology and Bioenergetics" (S. Papa, B. Chance, and L. Ernster, eds.), pp. 349–360. Plenum, New York, 1988.
77. Foote, N., Gadsby, P. M. A., Greenwood, C., and Thomson, A. J., *Biochem. J.* **261,** 515 (1989).
78. Wittenberg, J. B., *J. Biol. Chem.* **253,** 5694 (1978).
79. Gans, P., Buisson, G., Duée, E., Marchon, J.-C., Erler, B. S., Scholz, W. F., and Reed, C. A., *J. Am. Chem. Soc.* **108,** 1223 (1986).
80. Goff, H. M., and Phillippi, M. A., *J. Am. Chem. Soc.* **105,** 7567 (1983).
81. Foote, N., Gadsby, P. M. A., Field, R. A., Greenwood, C., and Thomson, A. J., *FEBS Lett.* **214,** 347 (1987).
82. Schulz, C. E., Devaney, P. W., Winkler, H., Debrunner, P. G., Doan, N., Chiang, R., Rutter, R., and Hager, L. P. *FEBS Lett.* **103,** 102 (1979).
83. Browett, W. R., Gasyna, Z., and Stillman, M. J., *J. Am. Chem. Soc.* **110,** 3633 (1988).
84. Ellfolk, N., Ronnberg, M., Aasa, R., Andreasson, L. E., and Vängård, T., *Biochim. Biophys. Acta* **743,** 23 (1983).
85. Foote, N., Peterson, J., Gadsby, P. M. A., Greenwood, C., and Thomson, A. J., *Biochem. J.* **230,** 227 (1985).
86. Foote, N., Thompson, A. C., Barber, D., and Greenwood, C., *Biochem. J.* **709,** 701 (1983).

87. Foote, N., Peterson, J., Gadsby, P. M. A., Greenwood, C., and Thomson, A. J., *Biochem. J.* **223,** 369 (1984).
88. Brunori, M., and Chance, B., eds., *Ann. N. Y. Acad. Sci.* **550,** 1–381 (1988).
89. Ludwig, B., *FEMS Microbiol. Rev.* **46,** 41 (1987).
90. Raito, M., Jalli, T., and Saraste, M., *EMBO J.* **6,** 2825 (1987).
91. Haltia, T., Puustinen, A., and Finel, M., *Eur. J. Biochem.* **172,** 543 (1988).
92. Steffens, G. C. M., Biewald, R., and Buse, G., *Eur. J. Biochem.* **164,** 295 (1987).
93. Yewey, G. L., and Caughey, W. S., *Ann. N. Y. Acad. Sci.* **550,** 22 (1988).
94. Holm, L., Saraste, M., and Wikström, M. *EMBO J.* **6,** 2819 (1987).
95. Martin, C. T., Scholes, C. P., and Chan, S. I., *J. Biol. Chem.* **263,** 8420 (1988).
96. Kroneck, P. M. H., Antholine, W. A., Riester, J., and Zumft, W. G., *FEBS Lett.* **242,** 70 (1988); **248,** 212 (1989).
97. Li, P. M., Malmström, B. G., and Chan, S. I., *FEBS Lett.* **248,** 210 (1989).
98. Saraste, M., Raitio, M., Jalli, T., Chefuri, V., Lenneux, L., and Gennis, R. B., *Ann. N. Y. Acad. Sci.* **550,** 315 (1988).
99. Salerno, J. C., Boligiano, B., Poole, R. K., Gennis, R. B., and Ingledew, W. J., *J. Biol. Chem.* **265,** 4364 (1990).
100. Eglinton, D. G., Hill, B. C., Greenwood, C., and Thomson, A. J., *J. Inorg. Biol.* **2,** 1 (1984).
101. Stevens, T. H., and Chan, S. I., *J. Biol. Chem.* **256,** 1069 (1981).
102. Hill, B. C., Brittain, T., Eglinton, D. G., Gadsby, P. M. A., Greenwood, C., Nicholls, P., Peterson, J., Thomson, A. J., and Woon, T. C., *Biochem. J.* **215,** 57 (1983).
103. Johnson, M. K., Eglinton, D. G., Gooding, P. E., Greenwood, C., and Thomson, A. J., *Biochem. J.* **193,** 699 (1981).
104. Jonson, P., Wilson, M. T., Aasa, R., and Malstrom, B. G., *Biochem. J.* **224,** 829 (1984).
105. Greenwood, C., Thomson, A. J., Barrett, C. P., Peterson, J., George, G. N., Fee, J. A., and Reichardt, J., *Ann. N. Y. Acad. Sci.* **550,** 47 (1988).
106. Cheesman, M. R., Turner, R., Greenwood, C., Thomson, A. J., and Reichardt, J., unpublished work.
107. Scott, R. A., Zumft, W. G., Coyle, C. L., and Dooley, D. M., *Proc. Natl. Acad. Sci. U.S.A.* **86,** 4082 (1989).
108. Farrar, J., Dooley, D. M., Zumft, W. G., Cheesman, M. R., and Thomson, A. J., unpublished work.